https://doi.org/10.5194/egusphere-2026-4850
Preprint. Discussion started: 20 August 2026

Comparing 3 m resolution snow cover downscaled from MODIS, VIIRS, and HLS using commercial satellite imagery and terrain information

Justin M. Pflug[1,2], Kehan Yang[3,2], Nicoleta Cristea[4,5], Emma T. Boudreau[4], Carrie M. Vuyovich[2], Sujay V. Kumar[2]

[1]Earth System Science Interdisciplinary Center, University of Maryland, College Park, College Park, Maryland, USA
[2]Hydrological Sciences Laboratory, NASA Goddard Space Flight Center, Greenbelt, Maryland, USA
[3]Science Systems and Applications, Inc., Lanham, Maryland, USA
[4]Department of Civil and Environmental Engineering, University of Washington, Seattle, Washington, USA
[5]eScience Institute, University of Washington, Seattle, Washington, USA

Correspondence to: Justin M. Pflug (jpflug@umd.edu)

Abstract. The fine scale distribution of snow is important for avalanche forecasting and biological refugia. Here, we test how historical context provided by 3 m snow cover observations derived from PlanetScope commercial satellite imagery could be used to downscale fractional snow covered area (fSCA) observed by the MODerate resolution Imaging Spectroradiometer (MODIS), Visible Infrared Imaging Radiometer Suite (VIIRS), and the Harmonized Landsat and Sentinel-2 (HLS) product using previously published approaches. We evaluate this over Colorado and California montane meadows using 1) probabilistic snow cover maps, and 2) random forest machine learning models. We then compare versus a downscaling benchmark that relies only on terrain characteristics, eliminating the need for PlanetScope observations. Provided these three approaches, downscaling snow cover using random forest models performed best on average, largely because these models corrected annually consistent snow cover biases between PlanetScope and coarser resolution fSCA observations. The approach used to downscale influenced 3 m snow cover most, followed closely by the accuracy of the fSCA estimate that snow cover was downscaled from. Snow cover downscaled from HLS using only terrain indices was often similar or better than snow cover downscaled from MODIS and VIIRS using context from PlanetScope. This demonstrates how a limited historical record of commercial satellite observations can be used to estimate the fine-scale pattern of snow cover in many regions, but also when publicly accessible remote sensing retrievals and information about the terrain may obviate the need for commercial observations.

1. Introduction

The fine scale distribution of snow is important for numerous hydrological, ecological, and risk-relevant human systems. For example, the distribution of deeper and shallower snow deposits and the resulting timing of snow disappearance has impacts on the abundance, species, resilience, and timing of blooming for a variety of plant species (Breckheimer et al., 2020; Ford et al., 2013; Litaor et al., 2008; Oldfather et al., 2024; Shirley et al., 2025). Snow heterogeneity drives variability in the timing of snowmelt onset and the exposure of glacier ice which can influence the late-season timing and volume of streamflow (Boardman et al., 2025; Brauchli et al., 2017; Dadic et al., 2010; Pfohl et al., 2026), soil thermal properties, and degradation of permafrost (Bisht et al., 2018; Krogh and Pomeroy, 2021). Information about the distribution of snow cover and snow structure at footprints relative to wind-driven snow redistribution and preferential deposition is also valuable for understanding snowpack

https://doi.org/10.5194/egusphere-2026-4850
Preprint. Discussion started: 20 August 2026

stability and risk of avalanches in mountainous terrain (Kronholm and Schweizer, 2003; Ortner et al., 2023; Schweizer et al., 2008).

The processes that drive fine-scale (< 10 m) snow distribution relevant for the applications above are complex and distinct from the information required to estimate average snow volume at coarser scales (Clark et al., 2011; Faria et al., 2000; Ford et al., 2013; Magoun et al., 2017; Mott and Lehning, 2010). To address snow at these scales, models have been developed to resolve complex processes like wind redistribution, saltation, preferential deposition, and canopy effects (Broxton et al., 2015; Lehning et al., 2006; Liston and Elder, 2006; Mazzotti et al., 2020). However, these models can be subject to process misrepresentations, and require accurate meteorological forcing at comparable resolutions, which is difficult to obtain in snowy, complex, and inaccessible terrain (Pflug et al., 2021; Reynolds et al., 2021). Manual observations of fine scale snow distribution are also challenged by the significant spatial heterogeneity of snow and hazardous conditions that can exist in many mountainous and arctic snowy environments. While remote sensing observations from platforms like airborne lidar are providing the capability to view snow distribution and snow cover at 3 m, or finer spatial resolutions (Kostadinov et al., 2019; Painter et al., 2016), this type of data is not available frequently, and at global scales.

Satellite remote sensing can be used to bridge the gap between snow model errors and the sparsity of in situ observations (Clark et al., 2006; Liu et al., 2013; Pflug et al., 2025; Yang et al., 2021). However, no publicly accessible snow cover remote sensing platform can currently observe the pattern of snow presence and absence at drift spatial scales (< 10 m). This has prompted the use of remote sensing retrievals from the commercial sector. For example, satellite retrievals from PlanetScope's (PS) commercial constellation of cube satellites have demonstrated the capability to resolve snow cover at approximately 3 m spatial resolutions in complex, unforested terrain (Cannistra et al., 2021; John et al., 2022; Yang et al., 2023). The 3 m pattern of snow cover in California and Colorado mountain meadows classified from PS using a random forest (RF) machine learning model had snow cover classification accuracies exceeding 85%, and when combined with nearby point observations of daily snow water equivalent (SWE), could be used to estimate 3 m and daily spring SWE evolution (Pflug et al., 2024). Despite this, PS remote sensing retrievals can be data intensive for large domains and time periods and require quality control and postprocessing procedures to convert raw data into snow cover maps.

Although challenging to observe, the fine scale pattern of snow in complex terrain is influenced by the interaction between prevailing winter and spring weather patterns and static features like the terrain and vegetation, meaning that spatial snow patterns often have some level of repeatability from one year to the next (e.g., Crumley et al., 2024; Deems et al., 2008; Mendoza et al., 2020; Pflug et al., 2024; Pflug and Lundquist, 2020; Schirmer et al., 2011; Sturm and Wagner, 2010; Vögeli et al., 2016; Woodruff and Qualls, 2019). This suggests that where similar snow cover patterns emerge annually, coarser-resolution remote sensing observations of fractional snow covered area (fSCA) could be related to the most likely underlying pattern of snow cover derived from commercial data from a limited number of retrievals in previous years. In doing so, the effort necessary to obtain and process fine resolution binary snow cover maps from commercial imagery could be limited and used to provide important context for free and easily accessible fSCA retrievals.

The concept of leveraging snow cover repeatability has been applied by previous studies. For example, snow depletion curves have been widely used to connect remote sensing estimates of fSCA over select regions with the underlying evolution of total snow mass (Liston, 2004; Luce and Tarboton, 2004; Shamir and Georgakakos, 2007). These relationships have been developed even further for assimilating and constraining process-based snow simulations (Andreadis and Lettenmaier, 2006; Clark et al., 2006; Margulis et al., 2015; Pflug et al., 2022). Repeatable snow patterns from previous years have also been used to connect snow cover observations over time, or at various scales, as the basis for downscaling or gap-filling in periods when

https://doi.org/10.5194/egusphere-2026-4850
Preprint. Discussion started: 20 August 2026

observations may not exist (e.g., Dong et al., 2020; Mahanthege et al., 2024; Premier et al., 2021b, 2021a; Revuelto et al., 2021; Rittger et al., 2021b; Woodruff and Qualls, 2019).

In this study, we investigate if observations of snow presence and absence from PS over a period from 2019 – 2023 could be used to downscale the 3 m distribution of snow cover from coarser-resolution fractional snow cover observed from the MODerate resolution Imaging Spectroradiometer (MODIS, ~500 m resolutions), Visible Infrared Imaging Radiometer Suite (VIIRS, ~375 m), and the Harmonized Landsat and Sentinel-2 (HLS, 30 m) product. We investigate this over seven mountain landscapes in Colorado and California (Fig. 1), performing a comparison of three previously published downscaling approaches. We begin by applying a downscaling approach that only uses information about the terrain (Cristea et al., 2017), assuming that the drivers of snow cover are annually repeatable. Using this downscaling approach as a benchmark, we then test a probabilistic method that weights the likelihood of fine scale snow cover using the frequency of snow cover from finer scale observations (Revuelto et al., 2021). We calculate these probabilities using PS snow cover, and in doing so, again assume annually repeatable drivers of snow cover that are observationally informed but not necessarily dependent on terrain characteristics. We finish by comparing a RF machine learning approach used to connect the coarser-scale fractional snow cover with the underlying 3 m PS snow cover maps and additional information about the terrain (Mahanthege et al., 2024). Relative to the approach using probabilistic weights informed from the same PS observations, this downscaling approach tests the extra value added by 1) the inclusion of terrain information, 2) the flexibility for the downscaling model to learn different connections across different regions, and 3) the ability to correct for annually persistent biases between snow cover observed from PS and coarser-resolution retrievals.

By comparing three previously developed snow cover downscaling approaches over seven domains, this comparison provides a glimpse of the context that historical PS observations can provide for snow cover estimates made at 3 m spatial resolutions. We ask three overarching questions:

1. Which of the three snow cover downscaling approaches performs best during spring snowmelt periods?
2. How much do PS snow cover maps from prior years improve 3 m downscaled snow cover maps, and is the terrain-based downscaling benchmark (without context provided by PS snow cover observations) able to perform similarly?
3. Which influences the relative accuracy of downscaled snow cover estimates more: a) the accuracy of the coarser resolution fSCA estimate from MODIS, VIIRS, and HLS; or b) the snow cover downscaling approach?

No other study has compared these downscaling approaches, nor have used them as the basis for inferring snow cover at 3 m spatial resolutions. This experimental design uniquely focuses on determining the degree to which downscaled snow cover estimates are altered by sensor accuracies, snow cover pattern references (either terrain-based or observationally based), and model architectures across seven different domains and four different years.

2. Domains and data

Snow cover observations at 3 m resolutions between 2019 and 2023 were accessed from Pflug et al. (2024). This data included seven montane meadows and ridgelines in California and Colorado (Fig. 1). Snow cover maps were processed using a random forest machine learning model adapted from Yang et al. (2023), informed from the red, blue, green, and near-infrared wavelengths from the PS constellation of Dove cube satellites (Dove Classic, Dove-R, and SuperDove) (Frazier and Hemingway, 2021). The random forest model was used to classify snow presence, snow absence, and image artifacts like sun glint provided training from a limited number of manual image classifications. Days with significant cloud coverage were excluded, and a post-processing procedure was used to correct sporadic snow cover misclassifications that could occur due to

https://doi.org/10.5194/egusphere-2026-4850
Preprint. Discussion started: 20 August 2026

off-nadir viewing angles, terrain-shading, and blocking by the forest canopy. Relative to airborne lidar observations, PS 3 m snow classifications were highly accurate, and the timing of snow disappearance was certain to within 3 days, on average. Readers are referenced to Pflug et al. (2024) for more information.

PS snow cover was used to both inform the pattern of 3 m downscaled snow cover and evaluate the accuracy of snow cover maps downscaled using coarser scale fSCA estimates from multiple sources. First, we used fSCA from NASA's MODerate resolution Imaging Spectroradiometer (MODIS), aboard the Terra and Aqua spacecrafts that were launched in 1999 and 2002, respectively. These observations provide daily estimates of fractional snow cover at ~500 m resolutions (Arsenault et al., 2014; Bennett et al., 2019; Gunnarsson et al., 2019; Hall et al., 2019) using an empirical relationship based on the Normalized Differential Snow Index (NDSI)(Hall et al., 1995; Salomonson and Appel, 2006, 2004). NOAA's Visible Infrared Imaging Spectroradiometer Suite (VIIRS), launched in 2011, has also been used to map daily snow cover at ~375 m spatial resolutions using a similar approach (Hall et al., 2019; Riggs et al., 2017; Rittger et al., 2021a). More recently, NASA's Harmonized Landsat and Sentinel-2 (HLS) project has provided the surface reflectance retrievals capable of calculating snow cover (Claverie et al., 2018). This product merges retrievals from both Landsat 8 and Sentinel-2 into a single product on a common 30 m grid with temporal repeats that can be as high as 2-3 days.

To ensure that fSCA observations were accessible on the same dates as PS snow cover observations, the MODIS and VIIRS fSCA estimates were accessed from the cloud-gap-filled products (Hall and Riggs, 2020; Riggs et al., 2019). These products provide time-continuous snow cover estimates by filling cloud-obscured pixels using the NDSI from the most-recent previous cloud-free observation. Because the HLS data does not currently include a snow cover product, we repeated the process used to estimate MODIS and VIIRS fSCA by 1) calculating the NDSI, 2) forward-filling NDSI in pixels and locations that were either obscured or within shadows cast by clouds (defined using HLS data quality flags), and 3) converting from NDSI to fSCA (Salomonson and Appel, 2006, 2004). It is important to note that while widely used for MODIS and VIIRS, this approach has not been explicitly tested for the HLS product to-date. For all three sensors, NDSI-based snow cover estimates are known to be biased by shadows, canopy coverage, atmospheric correction biases, and geolocation issues, particularly when derived at coarser resolutions and off-nadir angles that make snow cover between obstructing features more difficult to view (e.g., Aalstad et al., 2020; Arsenault et al., 2014; Raleigh et al., 2013).

Finally, two of the snow cover downscaling approaches tested in this study used information about the terrain and distribution of slopes with various pitches and orientations. These were derived from 3 m terrain elevation data from airborne lidar collected by the Airborne Snow Observatory (ASO)(Painter and Bormann, 2020) and the United States Geological Survey's 3D Elevation Program (3DEP)(Heidemann, 2012).

https://doi.org/10.5194/egusphere-2026-4850
Preprint. Discussion started: 20 August 2026

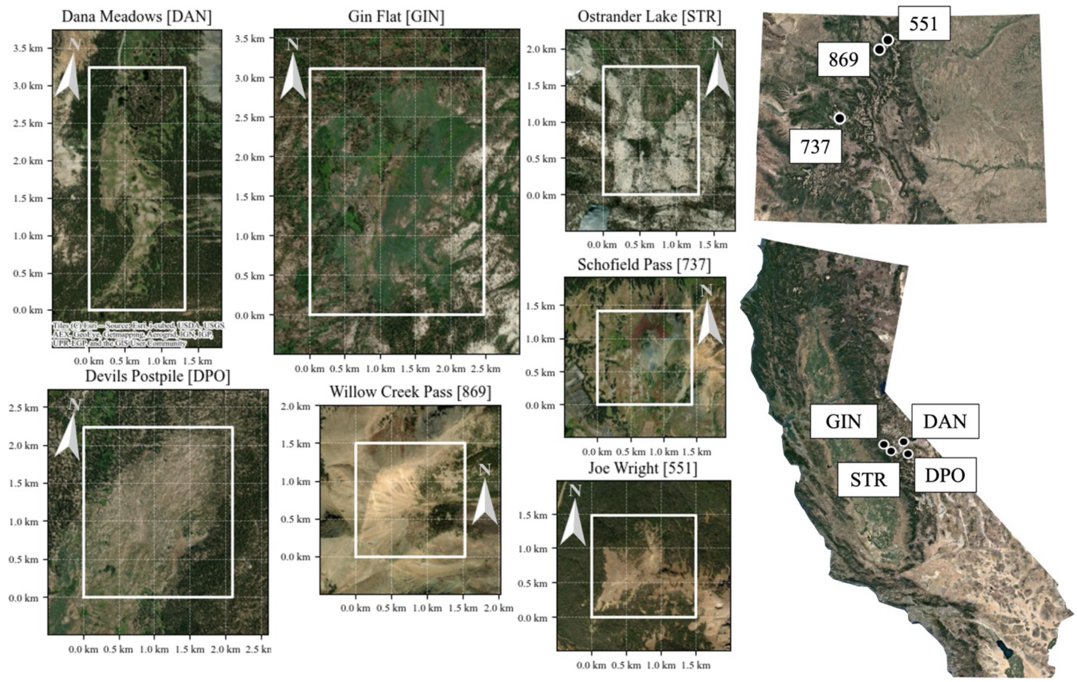

Figure 1. Model domains (white boxes), scaled by the approximate size of each domain, and named using the network ID from the nearest snow pillow (not pictured). Alphabetic names are in California (DAN, DPO, GIN, and STR), and numeric names are in Colorado (551, 737, and 869). While boxes delineate the total domain boundaries, snow cover downscaling was only performed in grid cells where PS observations were not obscured by canopy cover.

3. Methods

This study compared three snow cover downscaling approaches based on work by Cristea et al. (2017), Revuelto et al. (2021), and Mahanthege et al. (2024). In this section, we present the methods in order of increasing data requirements, advancing from snow cover downscaling using 1) terrain indices (Sect. 3.1), to 2) probability maps informed from PS snow cover observations (Sect. 3.2), and 3) RF machine learning approaches used to connect PS snow cover with the overlapping estimates of fSCA (Sect. 3.3) (Fig. 2). It is important to note that this is not a comprehensive selection of snow cover downscaling approaches available from the literature. Instead, these were chosen to focus on approaches that used many common inputs and progressed in a way that could be used to attribute the causes of changes to performance. This is discussed in-detail below (Sects. 3.1 – 3.3).

For each of the downscaling approaches, we derived 3 m estimates of binary snow presence and absence downscaled from MODIS, VIIRS, and HLS fSCA in water years 2019 – 2023. For methods that used PS observations to inform the downscaling, we used a leave-one-out approach, using PS snow cover maps from four years to downscale snow cover in a separate withheld year. For example, snow cover downscaled in 2022 used context from PS snow cover maps in 2019, 2020, 2021, and 2023. PS snow cover maps from 2022 were then used to validate downscaled snow cover. While using PS snow cover to both inform and assess the accuracy of downscaling risks propagating annually repeatable PS retrieval biases into both the model input and downscaling target, the high accuracy of these snow cover maps relative to airborne lidar observations make these retrievals a high benchmark for accuracy.

We measured the accuracy of downscaled snow cover maps versus PS observations in the withheld year using the weighted F1 score

https://doi.org/10.5194/egusphere-2026-4850
Preprint. Discussion started: 20 August 2026

$$F1_{score} = TP/[TP + \frac{1}{2}(FP + FN)], \quad (1)$$

where TP is the number of pixels with true positives, FP is the number of false positives, and FN is the number of false negatives. For each date, the F1 score is calculated twice, assuming that the goal is to predict snow presence (e.g., TP pixels have snow cover for both the downscaled snow cover and PS observation), and then snow absence. These F1 scores are combined using a weighted average based on the number of snow present and snow absent cells, respectively. This weighting decreases the sensitivity to misclassifications of snow cover for periods where only small portions of the domain are covered with snow. The resulting F1 score varied between 0 and 1, with 1 indicating a perfect classification for a single date at 3 m resolutions. Snow cover classification accuracy was also measured using Cohen's kappa

$$k = \frac{totalAccuracy - randomAccuracy}{1 - randomAccuracy}, \quad (2)$$

where,

$$totalAccuracy = \frac{TP+TN}{TP+TN+FP+FN}, \quad (3)$$

$$randomAccuracy = \frac{(TN+FP)*(TN+FN)+(FN+TP)*(FP+TP)}{(TP+TN+FP+FN)*(TP+TN+FP+FN)}, \quad (4)$$

and TN is the number of true negative classifications. k varies between -1 and 1, with 1 indicating a perfect classification. The use of random accuracy (Eq. 4) provides a comparison versus random guessing of snow presence and absence, standardizing against conditions with high and low amounts of snow cover.

A four-way Analysis of variance (ANOVA) was used to test the dependence of the F1 score and k variance on the downscaling approach, the sensor used to estimate fSCA that snow cover was downscaled from, the model domain, the year the downscaling occurred in (2019 – 2023), and all two-, three-, and four-way interactions between these categories. Put simply, this test measured how much of the total variability in these statistics could be described by each degree of freedom (e.g., the downscaling approach) as well as combined degrees of freedom (e.g., interaction between the sensor and downscaling approach) provided the limited number of sensors (3), downscaling approaches (3), domains (7), and years (5) tested here.

Finally, for each sensor and downscaling approach combination, the number of days with snow cover was summed for each 3 m grid. These were compared to the summed snow cover calculated from the PS data in each domain. The coefficient of determination (R^2) and percent-bias was used to measure the degree to which each downscaling approach and sensor resolved the 1) spatial pattern of spring snow persistence, and 2) overall biases in total snow coverage.

https://doi.org/10.5194/egusphere-2026-4850
Preprint. Discussion started: 20 August 2026

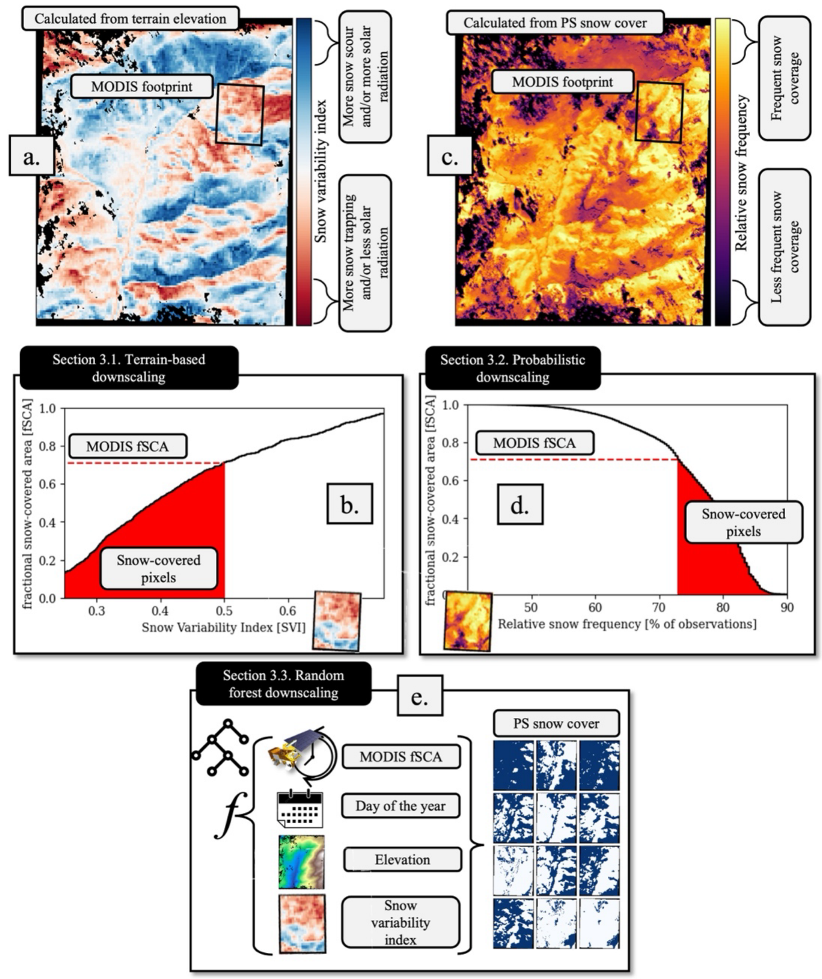

Figure 2. Conceptual diagram showing the snow cover downscaling procedure for all three approaches (black boxes), corresponding to the subsections below. This example shows the downscaling procedure for the area encompassed by a single MODIS footprint (box in the top two spatial plots) in the northeast portion of GIN that measures an fSCA of 0.71 on a single date.

3.1. Terrain-based downscaling

The first downscaling approach used topographic indices intended to represent the grid cells most likely to have enhanced snow accumulation, reduced snowmelt, and longer snow duration. This approach served as the downscaling benchmark; a measurement of the 3 m downscaling accuracy that could be achievable for midlatitude montane meadows only provided terrain elevation and assumptions of interannually repeatable drivers of snow accumulation and depletion. The terrain-based approach was based on Cristea et al. (2017), who showed that fractional snow covered area could be downscaled to finer resolution binary maps using a two-variable combined index, accurately matching snow distribution observed by lidar at 30 m spatial resolutions. The first component of this index was based on the diurnal anisotropic heat (DAH) index

$$DAH = \cos(\alpha_{max} - \alpha) \times \arctan(\beta), \quad (5)$$

where α is the terrain aspect, β is the slope angle (in radians), and α_{max} is the south southwest aspect that receives the maximum amount of daily solar cumulative radiation (202.5°). DAH spans -1 to 1 and indicates the grid cells with the least (DAH = -1) and greatest (DAH = 1) amount of solar incidence that could be available to melt snow. The second component is the topographic position index (TPI), which calculated the difference in elevation at every pixel (z_0), relative to the average elevation of the surrounding pixels ($\underline{z}$)

$$TPI = z_0 - \underline{z}. \tag{6}$$

This was used to identify grid cells with depressions (TPI < 0) where snow redistributed by wind, avalanching, or snow creep is more likely to increase snow accumulation. This is opposed to local maximas in the terrain (TPI > 0), where snow is less likely to be preferentially distributed and scour by wind may be increased.

The DAH (Eq. 5) and TPI (Eq. 6) were normalized between 0 and 1, and were combined to calculate the snow variability index (SVI) (Fig. 2a),

$$SVI = [w * DAH_{norm}] + [(1 - w) * TPI_{norm}], \tag{7}$$

where w is a tunable weighting factor that can be used to skew the SVI more towards spatially differential impacts on snow cover driven by snowmelt processes ($w > 0.5$) or snow accumulation processes ($w < 0.5$). Here, we tested SVI maps calculated from all combinations of 1) slopes and aspects calculated at three different spatial resolutions (3, 15, and 30 m), and 2) three unique w values (0.25, 0.5, and 0.75). This resulted in SVI maps that represented terrain-driven impacts on snow cover duration differently. For example, SVI calculated using a 3 m slope and aspect and an w of 0.25 assumed that the fine-scale ridges and depressions in the terrain would correlate in space with variabilities in snow distribution and the timing of snow disappearance. This combination also attributed the timing of snow disappearance more to the spatial variability in snow accumulation than the variability in snowmelt.

For each SVI map, we determined the 3 m pixels from PS observations with center points that were within each coarser-resolution footprint from MODIS, VIIRS, and HLS. Then, we ranked the underlying SVI values from lowest to highest, filling snow cover in that order until the fSCA estimate was matched (Fig. 2b). The 3 m elevation data was used as a secondary sorting criterion (ordered from highest to lowest elevation) where and when multiple pixels with the same SVI value spanned the number of pixels necessary to match MODIS, VIIRS, or HLS fSCA.

3.2. Probabilistic downscaling

The next downscaling approach used the relative frequency of snow cover observed from PS as the basis to identify the locations most likely to be covered by snow for any overlapping fSCA observation. This approach was motivated by Revuelto et al. (2021) who showed that the frequency of sub grid snow cover derived from Sentinel-2 could be used to downscale estimates of fSCA from MODIS to 20 m maps of snow distribution.

We tested the extent to which the probability of snow cover from four years could be used to downscale 3 m snow cover in a year withheld from the probability calculation. The probability of snow cover was calculated at each PS pixel as the frequency of snow cover observed at that location, divided by the number of PS observations (Fig. 2c). Snow cover was then increased in cells ordered from highest to lowest probability until fSCA was matched (Fig. 2d). Again, for instances where and when a single probability value corresponded to multiple grid cells, 3 m elevation was used as a secondary sorting criterion to determine the grid cells to prescribe as snow covered to match MODIS, VIIRS, and HLS fSCA.

This approach also assumed annually consistent drivers of snow distribution. It is functionally the same as the terrain-based downscaling benchmark (Sect. 3.2) but uses context from PS observations instead of terrain indices to inform the 3 m pattern of snow cover. Therefore, comparisons between this downscaling approach and the terrain-based downscaling provide measurements of the value provided by PS observations in other years.

https://doi.org/10.5194/egusphere-2026-4850
Preprint. Discussion started: 20 August 2026

3.3. Random forest downscaling

The final downscaling approach used a random forest (RF) machine learning model to determine the 3 m pixels most likely to be snow covered within any MODIS, VIIRS, and HLS footprint. This approach was motivated by Mahanthege et al. (2024) who demonstrated that a RF model could be used to downscale MODIS fSCA estimates to the spatial resolutions of less-frequent (~16 days), but higher-resolution (30 m) fSCA estimates from Landsat. Unique RF models were trained and performed across each individual MODIS, VIIRS, and HLS fSCA pixel. In other words, the number of RF models increased as the resolution of the fSCA estimate from each data source increased, and the number of pixels covering each study domain also increased. Again, a leave-one out approach was used, where the year the model was performed in was excluded from the model training.

The RF model inputs included the day of the year, 3 m elevation, and SVI (Sect. 3.1) (Fig. 2e). fSCA inputs were also included for each 3 m pixel coming from 1) the overlapping sensor footprint on the training/prediction date, as well as the prior and following dates, and 2) the fSCA across the full modeling domain on the training/prediction date. A minimum-maximum normalization was used to normalize all inputs between 0 and 1 except the fSCA time series, which was already restricted between 0 and 1. Minimum-maximum normalization was used instead of other standardization approaches in order to preserve the shape of the elevation and SVI distribution and thereby minimize differences between the inputs used for this downscaling approach and the terrain-based (Sect. 3.1) and probabilistic (Sect. 3.2) approaches. The models were then trained to predict the 3 m distribution of snow presence and absence observed by PS. Each model used 50 trees with a maximum depth of 20. However, RF snow cover classifications were insensitive to these parameters.

It is important to note that this approach and these inputs differ from the model developed by Mahanthege et al. (2024), who use models trained over larger subregions to predict continuous fSCA values between 0 and 1 using additional predictors like land cover type, latitude, longitude, forest height, barrier differences, distances to the ocean, and wind speed. However, the model inputs used here were chosen to correspond closely with the inputs used by the terrain-based and probabilistic downscaling approaches. Additionally, we focused our analysis only on PS snow cover maps from Pflug et al. (2024) which were across much smaller domains meaning that grid cell-level differences in latitude, longitude, barrier differences, and distance to the ocean were unlikely to drive meaningful differences in snow presence and absence. These PS snow cover maps also included only pixels without canopy coverage, meaning that forest height was also not an important predictor for this study. As noted above, we trained individual models at the footprint spatial extents of MODIS, VIIRS, and HLS observations, and therefore did not attempt to account for differences in terrain characteristics between different remote sensing footprints in the RF model.

The RF downscaling used PS snow cover context that was identical to the probabilistic downscaling approach (Sect. 3.2) but included the terrain information used by the terrain-based downscaling benchmark (Sect. 3.1). As opposed to the previous downscaling approaches, which ensured that the downscaled snow cover had fSCA equal to the coarser resolution estimate from MODIS, VIIRS, and HLS, the RF approach naturally adjusted the fSCA composed by the 3 m pattern of snow presence and absence based on the difference between PS snow cover and each of the fSCA data sources (MODIS, VIIRS, and HLS) from the model training. Therefore, comparisons of this approach and the probabilistic downscaling approach measure the value of terrain information and increased model flexibility, both with respect to correcting fSCA biases and downscaling algorithms that are allowed to vary for each coarse resolution fSCA footprint.

3.4. Random downscaling

https://doi.org/10.5194/egusphere-2026-4850
Preprint. Discussion started: 20 August 2026

To provide a baseline comparison for the terrain-based downscaling benchmark (Sect. 3.1), we used random grid cell assignments to classify the 3 m pixels with snow cover necessary to match fSCA from overlapping MODIS, VIIRS, and HLS footprints as closely as possible. This measured the value provided by 3 m terrain parameters (Sect. 3.1) without the benefit of PS observations from other years (Sects. 3.2 and 3.3). The random downscaling was compared only to the terrain-based downscaling. The accuracy of snow cover downscaled using random grid cell assignments is also analogous to the random accuracy metric (Eq. 4).

4. Results

4.1. Terrain-based downscaling parameter sensitivity

The pattern of 3 m snow cover downscaled using the terrain-based benchmark (Sect. 3.1) was sensitive to both the spatial resolution of the SVI, and the weighting factor (*w*). In GIN, 3 m SVI maps weighted to favor accumulation processes (*w = 0.25*) resulted in fine-scale variabilities in snow cover frequency, but less variability in snow duration across the domain as a whole (Fig. 3, top left). This parameter set implicitly reflected the terrain roughness. This was opposed to the snow cover downscaled using the 30 m SVI and 0.75 weighting factor, which prescribed differences in snow cover primarily to the 30 m pattern of solar exposure and resulting melt.

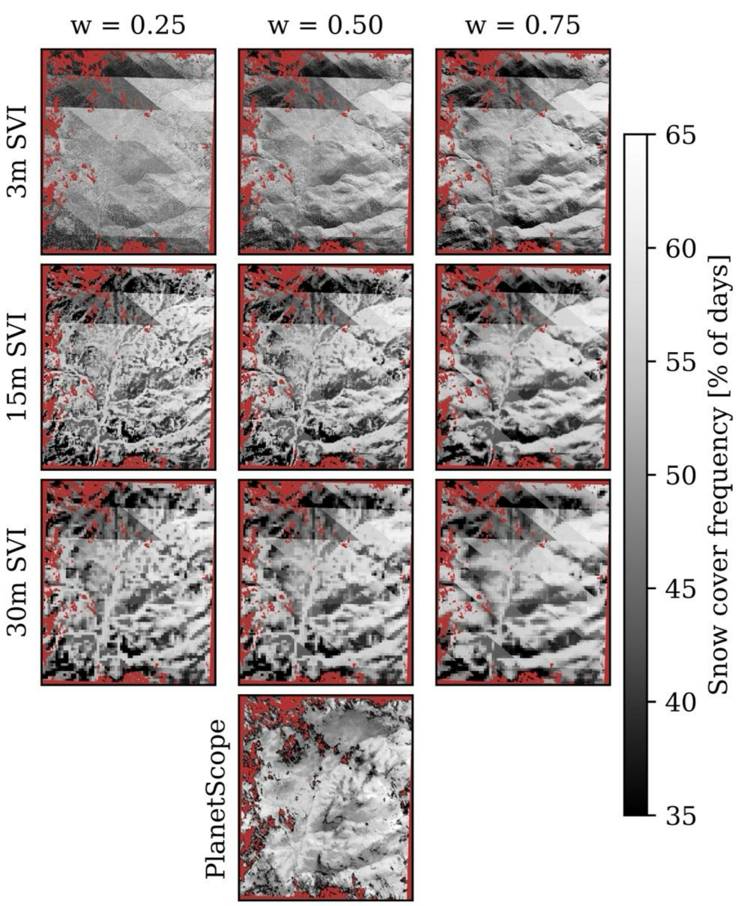

https://doi.org/10.5194/egusphere-2026-4850
Preprint. Discussion started: 20 August 2026

Figure 3. 3 m snow cover frequency on dates with PS snow cover observations (2019 – 2023) in GIN. Each estimate is downscaled using the terrain-based approach, fSCA from VIIRS, SVI maps at various resolutions (y-labels), and SVI maps using various weighting factors (top x-labels). Results are compared versus the 3 m pattern of snow cover frequency observed by PS (bottom subplot). Red pixels are locations that were unobserved by PS, either due to being outside the domain boundary or being blocked by canopy coverage or extreme slopes.

Comparisons versus PS snow cover (e.g., Fig. 3) determined that the terrain-based downscaling that used an SVI calculated at 15 m resolution, with a heavier weighting on the pattern of solar exposure (w = 0.75), had the best F1 scores (Eq. 1) and k (Eq. 2). This was true across both the GIN domain discussed above (Fig. 4a and Fig. S1a), and across all the study domains (Fig. 4b and Fig. S1b) for the three different fSCA retrievals. Conceptually, this meant that the pattern of snow disappearance observed from PS varied less from one 3 m grid cell to the next but instead had snow cover that disappeared at similar times as neighboring grid cells, the location and timing of which was described better by the pattern of solar exposure and shading than the distribution of depressions and uplifts in the terrain.

The accuracy of 3 m snow cover estimates downscaled using the terrain varied depending on the source of the fSCA estimate. In GIN, although the median F1 score only changed by less than 0.03 between the snow cover downscaled using MODIS and VIIRS fSCA, the disparity in the distribution of F1 scores between the different SVI resolutions and weighting factors was approximately 28% smaller when downscaling from VIIRS (Fig. 4a). In other words, downscaling snow cover from VIIRS fSCA instead of MODIS fSCA decreased the sensitivity to the SVI resolution and weighting factor. This was even more evident when downscaling snow cover from HLS fSCA, which had little visible difference in the pattern of snow cover (Fig. S2) and nearly identical F1 scores and k for the different SVI resolutions and weighting factors (Fig. 4a and Fig. S1a). In all following text, results and statistics for the terrain-based downscaling benchmark are for snow cover downscaled using only the 15 m SVI with a weighting factor of 0.75.

https://doi.org/10.5194/egusphere-2026-4850
Preprint. Discussion started: 20 August 2026

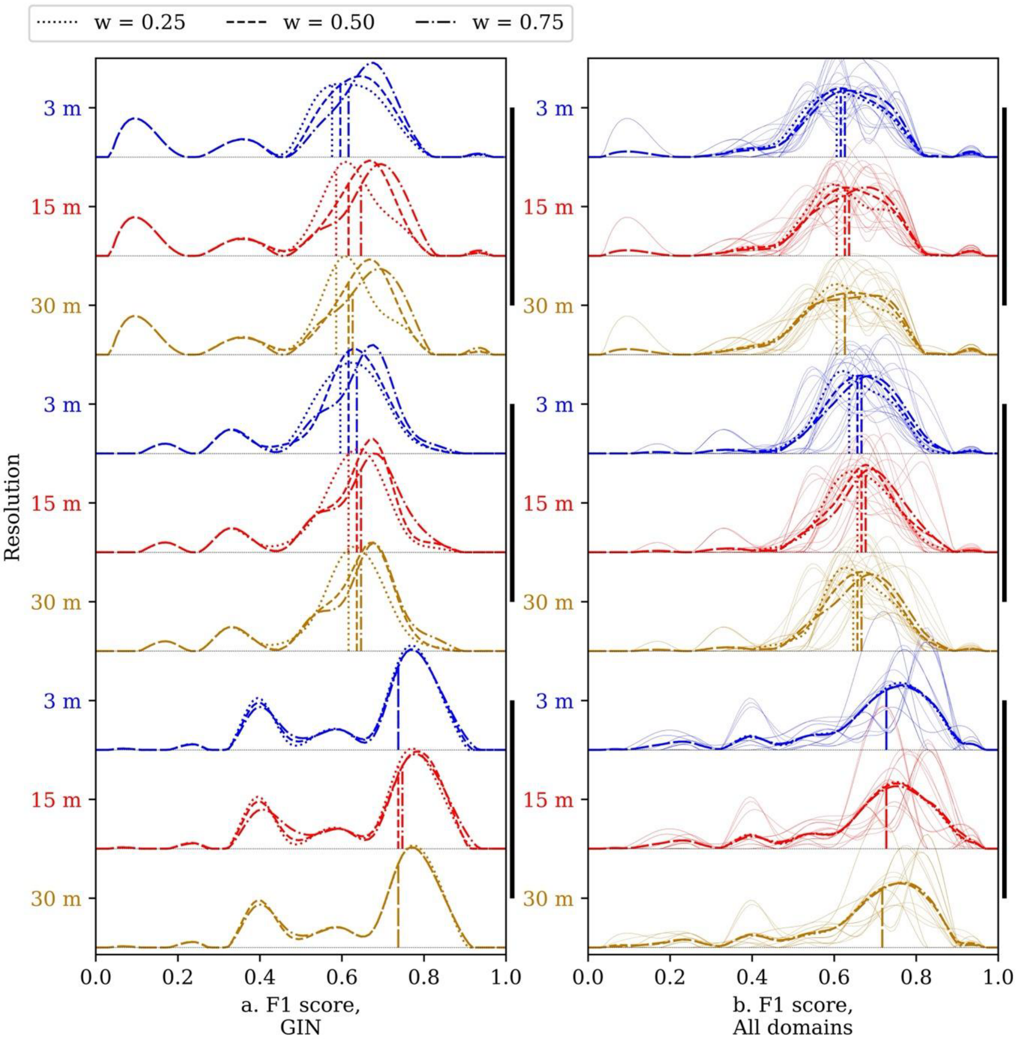

Figure 4. Distribution of the snow cover F1 score, relative to PS snow cover observations, including only dates when the domain-scale fSCA was between 0.15 and 0.85. Results include GIN (a, left) and all domains (b, right), and compare the performance of the terrain-based downscaling approach using three different fSCA datasets (right y-axis, black bars), SVI maps calculated at various resolutions (left y-axis and colors), and SVI maps using various weighting factors (line styles). Figure S1 shows the same results for the *k* statistic.

4.2. Snow cover downscaling comparisons

There was little difference to the accuracy of 3 m downscaled snow cover for the three different downscaling approaches tested here when evaluating versus the full record of observations (Fig. 5a). This was driven by the ~86% of the observations came from dates with conditions that had considerable snow coverage (domain-scale fSCA > 0.85; ~46% of the PS observation dates) or snow absence (domain-scale fSCA < 0.15; ~40% of the PS observation dates). On these dates, the F1 score and *k* was dictated almost entirely by whether the fSCA from MODIS, VIIRS, and HLS also resolved full or fully absent snow cover. The difference between the downscaling methods was much clearer for dates with transitional snow coverage, defined here as spring periods where the fSCA across the whole domain (as defined from PS) was between 0.15 and 0.85 (Fig. 5a). On these 358

https://doi.org/10.5194/egusphere-2026-4850
Preprint. Discussion started: 20 August 2026

dates, 3 m downscaled snow cover accuracy was influenced by 1) decisions made by each downscaling approach about where to assign 3 m snow presence and absence, 2) the accuracy of fSCA estimates from MODIS, VIIRS, and HLS (Fig. 5b and Fig. S3a), 3) the model domain (Fig. 5c and Fig. S3b), and 4) the year the downscaling occurred in. Results in the remainder of this manuscript focus on comparisons between downscaled snow cover maps versus the PS snow cover maps with domain-scale fSCA between 0.15 and 0.85.

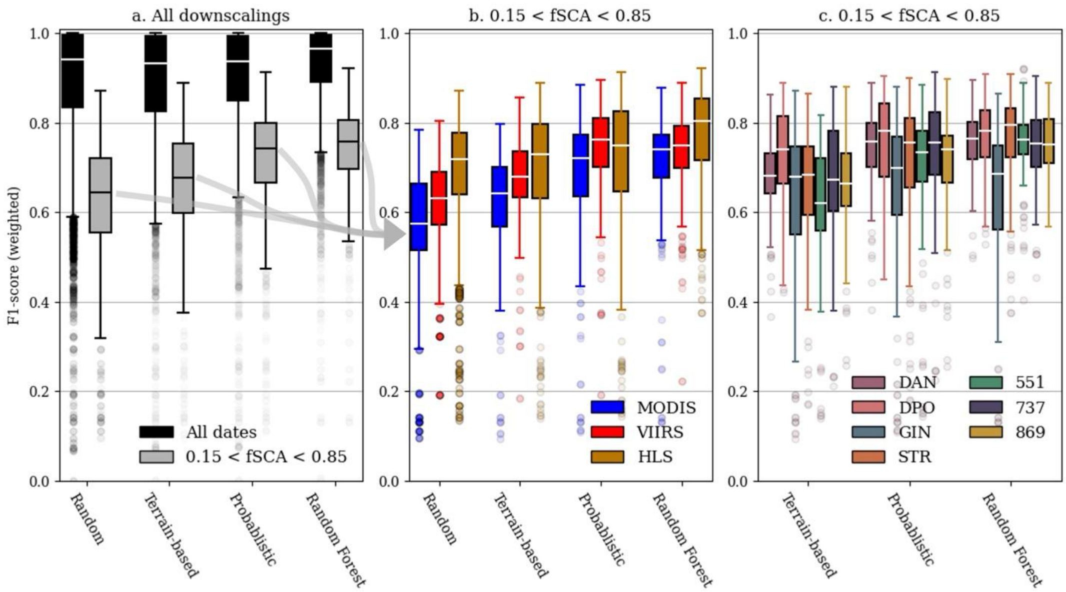

Figure 5. Distribution of F1 scores for 3 m downscaled snow cover maps versus PS snow cover observations. Subplot (a) compares F1 scores for all dates versus only dates with domain-scale fSCA between 0.15 and 0.85. The data from the gray boxplots in subplot (a) are then stratified by the source of the fSCA that estimates were downscaled from (b), and the domain (c). Similar plots for the *k* statistic can be found in Fig. S3.

Relative to random assignments of snow presence and absence (Sect. 3.4), the terrain-based downscaling benchmark only improved the snow cover F1 score from 0.64 to 0.68, on average (Fig. 5b). This was driven most by improvements to snow cover downscaled from MODIS (+0.07) and VIIRS (+0.05) fSCA (Fig. 5b and Table 1). The snow cover downscaled from HLS using the terrain-based approach resulted in only a 0.01 improvement to the median F1 score relative to the random pixel assignments. However, the pattern of mid-spring snow cover downscaled using this approach demonstrated some physically realistic characteristics. For example, snow cover downscaled from VIIRS fSCA on 29 June 2023 in DAN resolved more homogeneous snow cover in the eastern portion of the meadow, but patchier snow in the western portion of the meadow with snow disappearance occurring first on the elevated, southwestern side of hills (Fig. 6). This aligned with findings from Currier and Lundquist (2018) who measured significant differences in snow depth on the north and south-facing slopes over the same domain. However, DAN also contained a road in the west portion of the domain, where decreased albedo, increased ground heat fluxes, and plowing operations frequently resulted in spring snow absence. The terrain-based downscaling approach, which only used indices intended to connect the terrain aspect, slope, and ruggedness with the relative duration of snow cover, consistently assumed snow cover late into the snow season over this road.

The results above show that there was only minimal improvement for the terrain-based approach relative to random and uniformed assignments of snow presence and absence. Further, the relatively little change to the F1 scores between random and terrain-based downscalings from HLS suggested that the terrain provided little information about the preferential placement

https://doi.org/10.5194/egusphere-2026-4850
Preprint. Discussion started: 20 August 2026

of snow cover beyond what was already observed by the raw HLS retrievals. The remainder of the text compares the additional downscaling approaches relative to this terrain-based downscaling benchmark.

360 **Table 1. Median F1 score and the F1 score standard deviation (parentheses) for each combination of downscaling approaches and sensors in every domain, and averaged across all domains (rightmost column). Dark green cells indicate the best downscaling for each column, and light green cells indicate the second-best downscaling. The corresponding table for the *k* statistic can be found in Table S1.**

Downscaling	Sensor	DAN	DPO	GIN	STR	551	737	869	All doms.
Random	MODIS	0.62 (0.08)	0.61 (0.11)	0.55 (0.18)	0.54 (0.11)	0.56 (0.10)	0.56 (0.10)	0.60 (0.08)	0.57 (0.12)
	VIIRS	0.62 (0.07)	0.68 (0.07)	0.58 (0.12)	0.68 (0.06)	0.57 (0.09)	0.62 (0.07)	0.61 (0.08)	0.63 (0.09)
	HLS	0.69 (0.08)	0.80 (0.10)	0.74 (0.16)	0.71 (0.18)	0.62 (0.20)	0.78 (0.17)	0.70 (0.17)	0.72 (0.16)
Terrain-based	MODIS	0.68 (0.06)	0.66 (0.10)	0.64 (0.21)	0.59 (0.11)	0.61 (0.08)	0.58 (0.09)	0.66 (0.06)	0.64 (0.13)
	VIIRS	0.67 (0.07)	0.78 (0.06)	0.66 (0.15)	0.72 (0.05)	0.62 (0.08)	0.66 (0.06)	0.66 (0.08)	0.68 (0.10)
	HLS	0.70 (0.08)	0.83 (0.10)	0.75 (0.16)	0.73 (0.19)	0.63 (0.20)	0.80 (0.18)	0.71 (0.17)	0.73 (0.17)
Probabilistic	MODIS	0.75 (0.07)	0.67 (0.11)	0.67 (0.22)	0.66 (0.11)	0.78 (0.06)	0.72 (0.10)	0.74 (0.06)	0.72 (0.13)
	VIIRS	0.78 (0.08)	0.82 (0.05)	0.69 (0.14)	0.81 (0.05)	0.72 (0.07)	0.74 (0.06)	0.76 (0.08)	0.76 (0.10)
	HLS	0.72 (0.09)	0.84 (0.10)	0.76 (0.16)	0.75 (0.20)	0.65 (0.20)	0.83 (0.18)	0.72 (0.17)	0.75 (0.17)
Random forest	MODIS	0.75 (0.05)	0.73 (0.07)	0.66 (0.19)	0.73 (0.08)	0.75 (0.06)	0.74 (0.06)	0.74 (0.04)	0.74 (0.11)
	VIIRS	0.74 (0.07)	0.78 (0.07)	0.70 (0.12)	0.81 (0.05)	0.75 (0.07)	0.73 (0.06)	0.76 (0.04)	0.75 (0.09)
	HLS	0.81 (0.07)	0.84 (0.09)	0.70 (0.12)	0.82 (0.15)	0.79 (0.09)	0.82 (0.11)	0.81 (0.09)	0.80 (0.11)

https://doi.org/10.5194/egusphere-2026-4850
Preprint. Discussion started: 20 August 2026

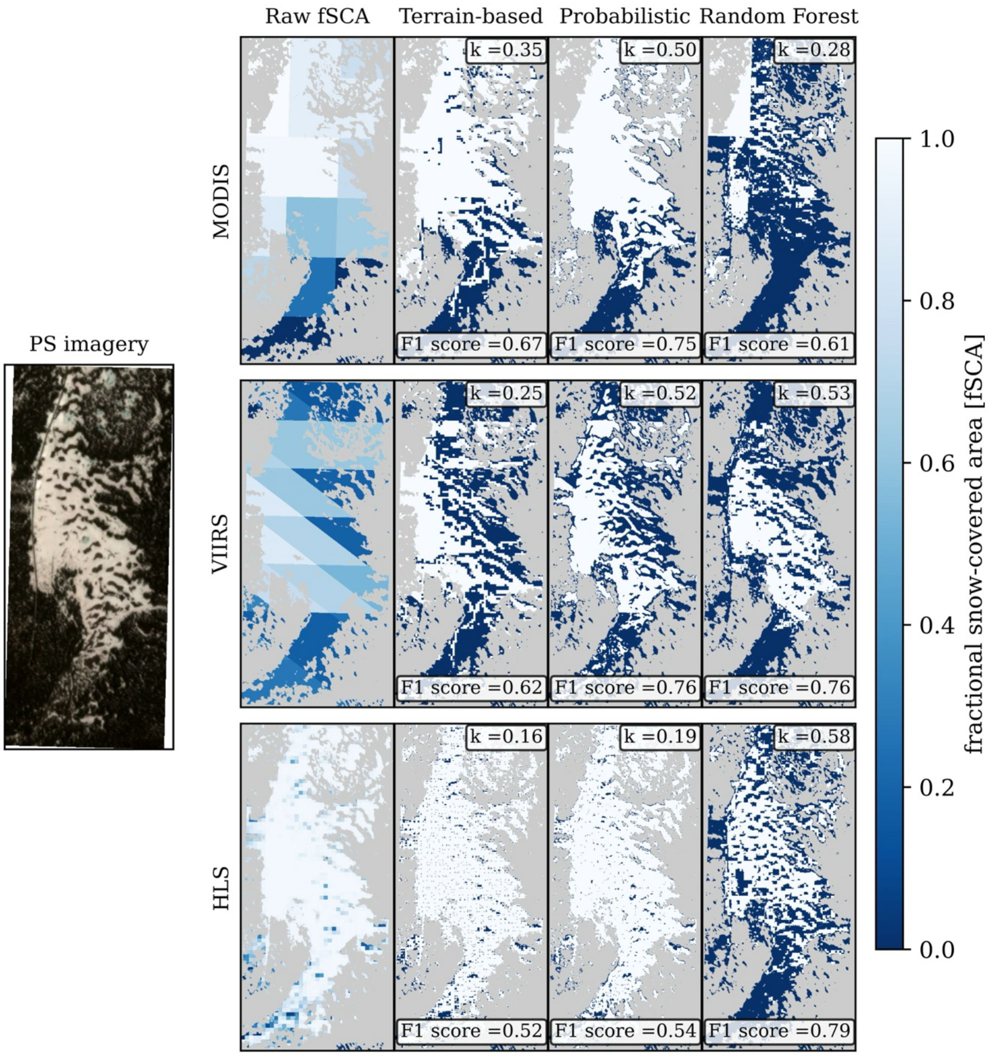

Figure 6. Comparisons of 3 m snow cover downscaled from MODIS, VIIRS, and HLS fSCA on 29 June 2023 in DAN. For visual context, PS true-color imagery for this date is also provided.

Including historical context from PS snow cover improved the accuracy of the 3 m snow cover downscaling in each domain (Fig. 5b and Fig. S3). In fact, provided the three downscaling approaches and three sensors tested here, every domain's best-performing downscaling approach used PS snow cover maps (Table 1 and Table S1). Relative to the benchmark provided by the terrain-based downscaling approach which used the same method but the terrain as a reference for downscaling, the probabilistic downscaling approach (Sect. 3.2) improved the median F1 score by 0.06 (9%) and the median k by 0.17 (85%). When stratifying the change in performance by sensor, snow cover downscaled from MODIS fSCA had the greatest improvements (F1 score improved 0.08, *k* improved 0.15), followed by VIIRS (F1 score improved 0.07, *k* improved 0.17), and then HLS (F1 score improved 0.03, *k* improved 0.05). Results were similar for the RF downscaling approach (Sect. 3.3), which improved the F1 score by 0.09 (13%) on average, with a 0.10, 0.07, and 0.06 F1 score improvement when downscaling from MODIS, VIIRS, and HLS fSCA, respectively. The RF downscaling approach improved the *k* statistic by 0.19 (95%) on average, with a 0.16, 0.12, and 0.14 improvement when downscaling from MODIS, VIIRS, and HLS.

https://doi.org/10.5194/egusphere-2026-4850
Preprint. Discussion started: 20 August 2026

Of the seven domains investigated here, four domains (DAN, DPO, 551, and 869) had the best overall F1 scores and k statistics when downscaling 3 m snow cover using the RF downscaling approach (Fig. 5c, Fig. S3b, Table 1, and Table S1). The RF approach improved performance relative to the probabilistic approach most by bias-correcting the downscaled snow coverage based on the historical context learned from disparities between PS snow cover and fSCA from each sensor. For example, in DAN, the RF downscaling learned that fSCA from both MODIS and HLS tended to overestimate snow cover as compared to the PS observations (Fig. 6). Relative to the terrain-based and probabilistic approaches, which assigned the number of snow covered pixels necessary to match fSCA from the overlying satellite footprint (Fig. 2), the RF approach learned to reduce snow in the locations that PS most-frequently observed snow absence. In DAN, this ended up improving the HLS median F1 score by 0.09 and median k by 0.18, relative to the probabilistic downscaling approach.

The interactions between the different sensors (MODIS, VIIRS, and HLS) and downscaling approaches discussed above had clear impacts on the spatial pattern of snow persistence in each domain (Fig. 7, Figs. S4 – S9). For example, in Schofield pass (domain 737), fSCA from MODIS and VIIRS downscaled using the terrain-based approach had median snow persistence that agreed with PS observations (Fig. 7). However, the pattern of snow cover frequency was too spatially homogeneous and had significant low biases for a portion of the domain, resulting in overall poor spatial patterns ($R^2 \leq 0.06$) and average biases between -4% and -15%. Downscaling using the probabilistic approach improved the R^2 of snow persistence patterns by 0.47 and 0.58 for the MODIS and VIIRS fSCA estimates, respectively, as these approaches better resolved the explicit placement of 3 m cells more and less likely to retain snow late into the spring snowmelt season. However, the average bias persisted between the terrain-based and probabilistic approaches. Spatially, these biases were located nearby scattered forest stands and ridges (Fig. 7, spatial plot), where impacts like terrain shading, obstructions from the canopy cover, viewing angle issues, and geolocation issues are known to drive fSCA errors (Arsenault et al., 2014; Raleigh et al., 2013; Rittger et al., 2021a; Stillinger et al., 2023). The random forest approach improved these fSCA biases and resulting pattern of snow persistence to within 2% for both MODIS and VIIRS. These results were similar for downscalings from the HLS fSCA but were generally less dramatic as the initial pattern of snow persistence for this sensor was captured better prior to downscaling.

https://doi.org/10.5194/egusphere-2026-4850
Preprint. Discussion started: 20 August 2026

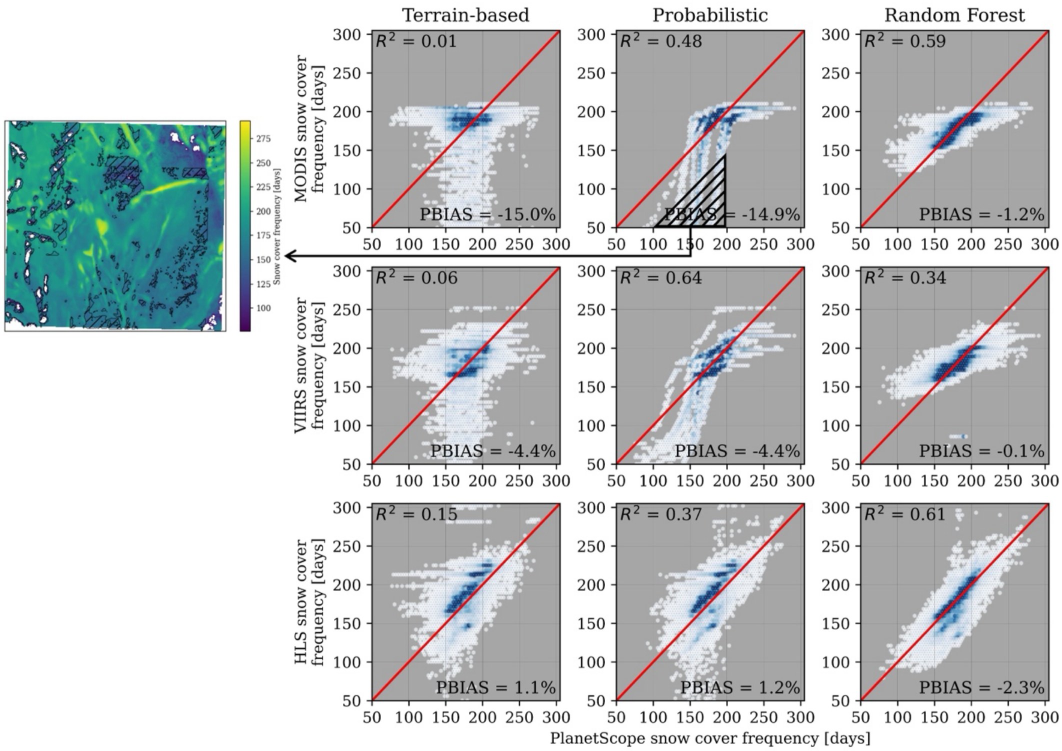

405 **Figure 7. 3 m snow cover frequency in 737 (Schofield Pass) from each sensor (rows) downscaled using the terrain-based, probabilistic, and random forest approaches (columns) compared to PS snow cover frequency (x-axes). Blue areas represent areas with higher point density. The pattern of snow cover frequency observed from PS is shown by the spatial plot, with hatched cells representing regions with the most significant biases when downscaling MODIS fSCA using the probabilistic approach.**

4.3. Individual and combined impact of downscalings, sensors, domains, and years

The four-way ANOVA test determined that the combined impact of the domain and year explained the greatest proportion of the variance in the F1 scores. This was followed closely by the downscaling approach in isolation. In other words, although the downscaling approach was a major driver of the accuracy of downscaled 3 m snow cover maps (Fig. 5 and Table 1), the degree to which the different downscaling approaches altered the F1 score varied based on the domain (Fig. 5c) and year (Fig. 8). This could be driven in part by dissimilarities in sensor accuracies and snow cover patterns from domain to domain. For example, using the same PS snow cover data, Pflug et al. (2024) noted that water-year 2019 was an average-to-high snow year in both California and Colorado that had snow disappearance patterns that were less correlated to the other years in the PS record (2020 – 2023). Here, snow cover downscaled using the probabilistic and RF approaches in 2019 using PS patterns from 2020 – 2023 tended to be slightly less accurate than the snow cover downscaled in the other years (Fig. 8). Conversely, snow cover downscaled by the terrain-based benchmark, which did not rely on historical context from PS, performed similarly or better in 2019 than in the other years.

Averaged across all sensors and downscaling approaches (excluding the random downscaling), the F1 scores varied between 0.50 (GIN in 2019) and 0.75 (DPO in 2022). This spread was more than 3 times larger than the change in performance between the terrain-based (0.66) and random forest (0.74) downscalings, when averaging across all dates, domains, and sensors. The k statistic tended to be more sensitive to downscaling approach (Fig. S3), meaning that the variance in this statistic was explained

https://doi.org/10.5194/egusphere-2026-4850
Preprint. Discussion started: 20 August 2026

almost equally by differences across years and domains, and different downscaling approaches. However, these results still demonstrated that 1) the choice of the downscaling approach had a significant impact on the F1 score and *k*, 2) 3 m snow cover generally improved when moving from the terrain-based, to the probabilistic, and finally to the random forest downscaling approach, but 3) variabilities in the F1 scores and *k* values existed from year to year and across the different domains.

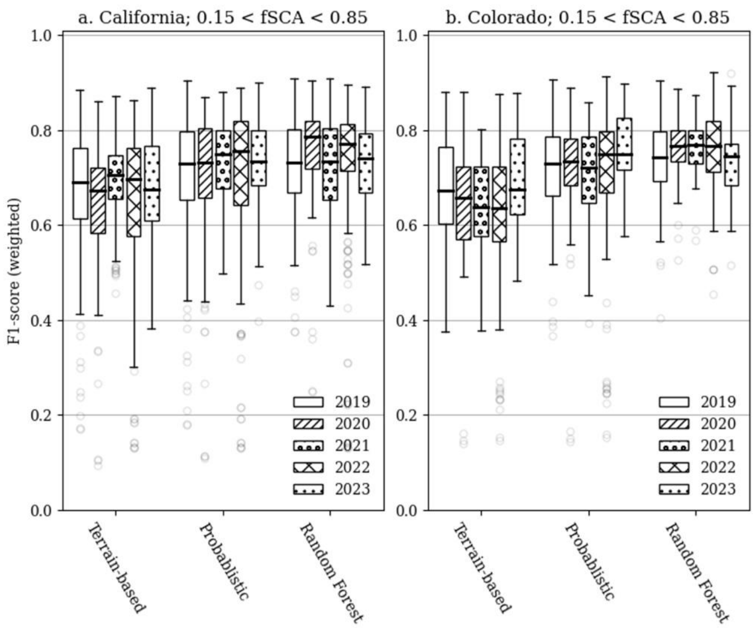

Figure 8. F1 score of snow cover downscaled using various approaches (x-axis), stratified by year (boxes) and by region (subplots). Subplots compare performance across California (a) and Colorado (b) domains.

Behind the domain, year, and downscaling method, the sensor that snow cover was downscaled from was the next-strongest descriptor of variances to both the F1 score and *k* statistic. In fact, the change in the F1 score only varied between 0.65 and 0.71 for MODIS and HLS, respectively, when averaging across all domains, years, and downscaling approaches. Figure 5b shows that for each downscaling approach, the median F1 score typically increased with the resolution of the fSCA observation. The exception was for the probabilistic approach, where the median F1 score was 0.01 better, and the F1 score standard deviation was 0.07 better, when downscaling snow cover from VIIRS fSCA instead of HLS fSCA. This was driven most by results in DAN, STR, and 551, which had spring domain-scale fSCA biases that were generally better for VIIRS than HLS (Fig. S10 – S12). This showed that the accuracy of fSCA estimates for each sensor changed across the domains, likely as a function of the complexity of the terrain and degree to which remotely sensed snow cover was biased by impacts from vegetation, viewing geometries, and shadows (e.g., Aalstad et al., 2020; Bair et al., 2023; Liu et al., 2020; Painter et al., 2009; Raleigh et al., 2013; Sirguey et al., 2009; Xin et al., 2012).

5. Discussion

The results show that the 3 m distribution of snow can be downscaled from coarser-resolution estimates of fSCA during spring snowmelt periods with the best-performing approaches spanning F1 scores of 0.76 to 0.84 and *k* values between 0.39 and 0.57. These accuracies are slightly worse than those reported by the studies that each downscaling approach was derived from (Cristea et al., 2017; Mahanthege et al., 2024; Revuelto et al., 2021). This was expected since we evaluated snow cover

https://doi.org/10.5194/egusphere-2026-4850
Preprint. Discussion started: 20 August 2026

downscaled to much finer spatial resolutions (3 m) than have been tested by any other study to date. Snow cover maps across smaller mountain meadows were influenced by complex processes like wind redistribution and microtopographical shading to a greater degree than effects like the elevation-driven seasonal snow lines, which are easier to observe from coarser remote sensing observations. While the accuracy of downscaled snow cover varied by the domain and year, accuracies generally increased with increases to the informative power of the inputs used for the three downscaling approaches tested here. This varied from terrain information only, to historical probabilities of snow cover likelihood, to historical context about snow cover patterns and the departure between the amount of snow cover observed by PS and each sensor. While we focused on small meadow domains, all three downscaling approaches were computationally inexpensive to perform. The process of obtaining and processing historical PS snow cover maps (Pflug et al., 2024) could be a bigger bottleneck for downscaling snow cover than the selection of the downscaling approaches tested here.

In this section, we expand on the results, investigating the spatial autocorrelation of snow cover patterns (Sect. 5.1), and the computational, economical, and performance benefits and tradeoffs for the three snow cover downscaling approaches (Sect. 5.2). We finish by attributing the dominant drivers of differences between the downscaling approaches (Sect. 5.3) and addressing study limitations and future recommendations (Sect. 5.4).

5.1. Spatial autocorrelation of snow cover

The slight improvement in performance for the terrain-based downscaling benchmark using SVI maps at 15 m resolutions, as compared to finer resolutions (Fig. 3 and Fig. 4), suggested that the terrain features responsible for controlling the accumulation and melt of snow, were at spatial lengths coarser than the 3 m PS resolution, on average. To test this, we calculated a semivariogram in each domain, measuring the degree of dissimilarity in the snow cover persistence at various distances (Fig. 9). Results found that the spatial disparity in the frequency of snow cover increased nearly linearly for distances between approximately 9 m and 60 m, beyond which increases were more gradual. This represented a “scale break” or “process-length” wherein the processes that drove the pattern of snow cover differed when observed at the resolutions on either side of the change in slope. Conceptually, the distance just before the variogram starts to flatten represents the coarsest spatial resolution that could realistically observe a large portion the snow cover pattern variability since snow cover at resolutions below this distance have some level of spatial autocorrelation.

All of the domains exhibited a change to the slope of the semivariance at distances between 30 m and 60 m (Fig. 9). This corresponds closely with studies that have documented scale breaks in snow depth and snow cover between 10 m and 60 m (Blöschl, 1999; Clark et al., 2011; Currier and Lundquist, 2018; Deems et al., 2006; Helbig et al., 2021; Helfricht et al., 2014; Mendoza et al., 2020; Miller et al., 2022; Pflug and Lundquist, 2020; Schirmer et al., 2011; Trujillo et al., 2009, 2007). Since 30 m distances corresponding to the resolution of HLS fSCA were commonly within the scale break and at low semivariances, this shows that HLS was often capable of viewing the pattern of snow cover from PS much more explicitly than MODIS or VIIRS. In other words, relative to MODIS and VIIRS, individual HLS footprints 1) viewed total or nearly full (fSCA near 1.0) or snow absent (fSCA near 0.0) conditions more frequently, and 2) had adjacent pixels that were more likely to exhibit similar fSCA values. This reduced impact of the snow cover downscaling approaches. This was opposed to footprints covered by MODIS and VIIRS pixels, which were more likely to have fSCA values that averaged variable snow cover over larger regions, meaning that subgrid information about the likelihood of snow cover was more valuable. While the goals of this study were to downscale snow cover to 3 m resolutions, the spatial autocorrelations also suggests that a lot of the snow cover information

https://doi.org/10.5194/egusphere-2026-4850
Preprint. Discussion started: 20 August 2026

could be captured by downscaling to resolutions coarser than PS observations using HLS snow cover if 30 m snow cover is sufficient (e.g., Figs. S14 and S15).

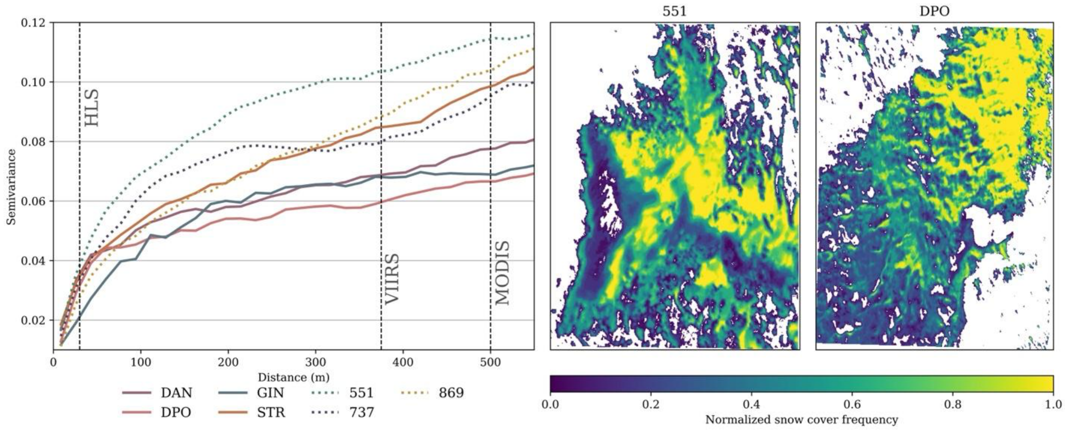

Figure 9. Spatial variogram of snow cover frequency (left). Vertical lines correspond to the resolution of each sensor used in this study. Spatial plots show examples of the normalized snow cover frequency for the 551 and DPO domains.

Overall, our findings suggested a higher frequency of full snow cover or total snow absence at fine (30 – 40 m) resolutions as compared to a similar study by Selkowitz et al. (2014). We anticipate that this may have been driven by 1) the domains focused on here which typically had less complex terrain, and 2) that binary snow presence and absence was calculated at coarser resolutions than the 0.5 m reference snow cover used by Selkowitz et al. (2014). We also recognize that we focused only on exposed areas since PS snow cover retrievals were blocked by the canopy overstory. However, differences in the timing of snow cover disappearance can occur over very small distances with changes in vegetation (Ford et al., 2013) and landcover, which can drive processes like ground heat fluxes, longwave emission, wind sheltering, and surface albedo feedbacks. While we focused on open meadows, to ensure that snow cover downscaling was not impacted by landcover, we assessed the weighted F1-score discretized by 10 m-resolution landcover classes defined from the ESA WorldCover product (Zanaga et al., 2022). Overall, there were no consistent changes in the performance of downscaled snow cover maps across different land cover types (Figs. S16 and S17).

5.2. Tradeoffs between model data requirements and practical benefit

The F1 score and *k* statistic used to measure the general performance for each sensor and downscaling combination across different domains and periods of time may not have a linear relationship with any single application. For example, a change in the F1 score of approximately 0.10 for moderate F1 scores (0.30 to 0.60) can indicate a significant change to the domain-scale determination of total snow coverage, important for applications like land-atmosphere feedbacks and land surface temperature. Smaller changes about larger F1 scores (e.g., 0.75 $\pm$ 0.05) could indicate smaller changes to total snow cover, but better determinations of fine-scale snow patterns, which could be more important for smaller-scale applications like wildlife denning habitat and avalanche forecasts.

To identify meaningful increases to the F1 score for the specific sensors and downscaling approaches tested here, we used the 75th percentile of F1 scores from the downscaling approach that used random pixel assignments as a threshold. Provided fSCA from MODIS and VIIRS, and the seven domains and years investigated here, the probabilistic and RF downscaling approaches improved the median F1 score beyond this threshold (Fig. 5b). For HLS, only the RF downscaling resulted in an

https://doi.org/10.5194/egusphere-2026-4850
Preprint. Discussion started: 20 August 2026

increase to the F1 score beyond the random pixel 75th percentile. For none of the sensors did the terrain-based downscaling increase the median F1 score beyond the 75th percentile of the random pixel downscaling.

The distributions in Fig. 5 were also used to identify downscaled snow cover maps with outlying poor performance. Overall, the worst-performing downscalings were driven by a combination of fSCA biases and the assumption of annually repeatable snow cover patterns used by each downscaling approach. For example, in GIN, fSCA from VIIRS sometimes had low biases exceeding 0.40, relative to PS. These biases were most focused in the northeastern portion of the domain where the VIIRS footprints overlapped significant forest cover and steeper slopes, potentially reducing the quality of retrievals and causing sharp discontinuities in the frequency of snow cover in these areas relative to the meadow (Fig. 3). The terrain-based downscaling benchmark had the lowest F1 scores on dates where these VIIRS biases were the most significant (Fig. S18). However, because these fSCA biases appeared frequently, the random forest model learned to partially correct these biases, showing much less of a relationship between the fSCA bias and F1 score. Pflug et al. (2024) also found that GIN had less interannual repeatability in the pattern of snow disappearance than the other domains. This appeared to influence the F1 scores for both the probabilistic and random forest approaches (Fig. S18) which relied on historical context from PS snow cover. While most notable in GIN, these effects appeared in other domains. For example, high-biased HLS early spring snow snow cover in DAN resulted in poor terrain-based and probabilistic downscalings, but was adjusted and corrected for by the random forest model (Fig. 6).

To provide more context for the utility of PS observations, we compared the 3 m snow cover frequency between 1) the best-performing snow cover downscaling approach that required no historical information from PS (HLS downscaled using the terrain-based approach), and 2) the best-performing snow cover downscaled using PS (Fig. 10). This comparison isolated the difference in 3 m snow cover when downscaled using only a single publicly accessible snow cover observation and a simple statistical approach, versus downscalings informed by PS commercial satellite imagery. The average error in snow cover frequency was 4 days better, and the spatial pattern of the snow cover frequency had a coefficient of correlation that was 0.29 better, and the coefficient of determination was 0.57 better for snow cover downscaling approaches using PS observations than downscaling from HLS fSCA using the terrain-based approach. Again, this improvement was driven predominantly by the random forest approach, which learned where and when snow cover from HLS tended to be biased as compared to PS. Additionally, snow cover downscaled from HLS using the terrain-based approach often had a speckled pattern of grid cells with reduced snow cover (Fig. 10). This was driven by a relatively large frequency of HLS fSCA pixels that estimated substantial snow cover, but fSCA that was still less than 1.0. As opposed to the RF approach that learned where and when these pixels were actually likely to be fully snow-covered, the terrain-based approach was limited to downscaling the snow cover to match the HLS fSCA, resulting in scattered 3 m grid cells that rarely had snow cover.

https://doi.org/10.5194/egusphere-2026-4850
Preprint. Discussion started: 20 August 2026

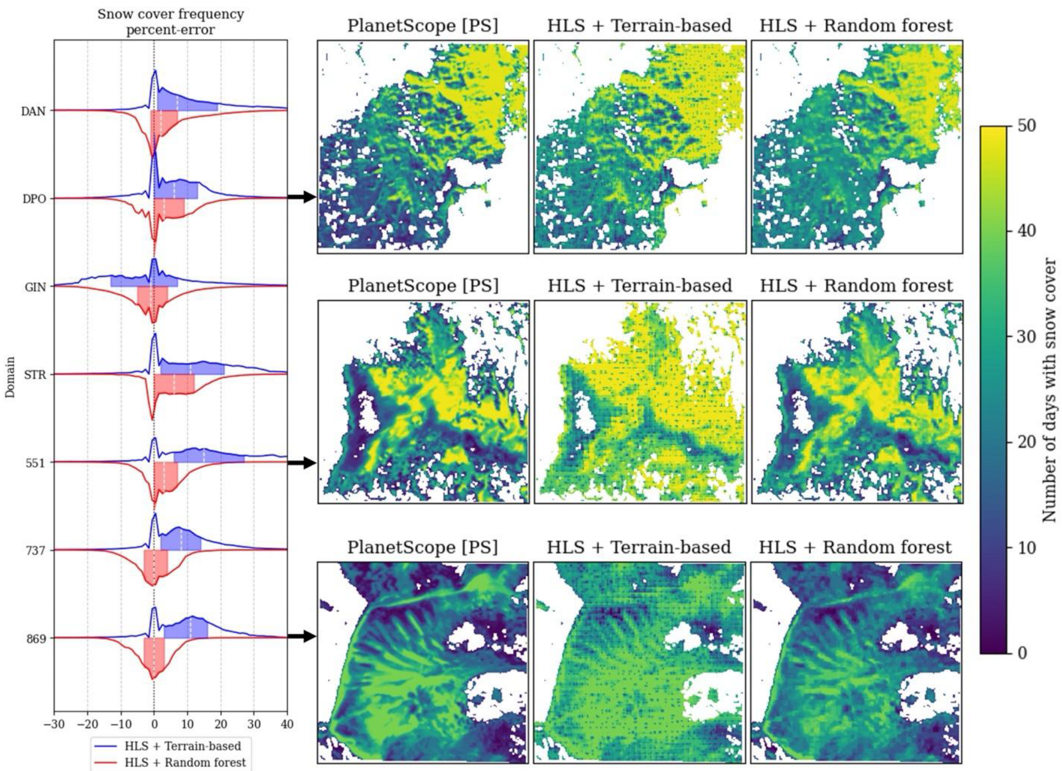

Figure 10. The frequency of snow cover at each 3 m pixel, as calculated by PS, HLS downscaled using the terrain-based downscaling, and HLS downscaled using the RF downscaling (spatial plots) for DPO (top), 551 (middle), and 869 (bottom). Distributions (left) show the relative frequency of the snow cover percent-error (x-axis) for each downscaling, relative to PS observations, with the shading representing the IQR and the dashed line representing the median.

The best approach for estimating 3 m snow cover may depend on the application and tradeoff between the economic and computational cost of accessing and processing commercial snow cover data and the practical benefit of fine-scale snow cover estimates. Since the pattern of snow presence and absence had levels of spatial autocorrelation at footprints comparable to the 30 m resolution from HLS (Fig. 9), HLS fSCA downscaled using only terrain indices often had similar or better performance than snow cover downscaled from coarser resolution fSCA (MODIS and VIIRS) using PS observations from other years (Fig. 5b). While Fig. 10 demonstrates how PS information could be used to correct HLS fSCA biases that were annually persistent, it is also possible that the limited number of years used in the model training could risk overfitting, resulting in the elimination or smoothing of true instances of sporadic snow presence and absence that could actually occur.

5.3. Attribution of downscaling performance changes

The terrain-based benchmark and probabilistic downscaling approach both assumed annually repeatable spring snow cover. Therefore, changes to the F1 score and k (Fig. 5 and Table 1) were driven only by a change to the 3 m pattern used for downscaling from terrain indices to explicit observations of 3 m snow cover in other snow years. In domains where snow cover patterns exhibited less annual repeatability (Sect. 5.2), the assumption of static snow cover patterns may have decreased performance. We hypothesize that a larger record of PS historical observations may be able to provide context from a wider range of years with variable snow conditions, and additional meteorological information, such as annual temperature and

https://doi.org/10.5194/egusphere-2026-4850
Preprint. Discussion started: 20 August 2026

precipitation anomalies, could be used as the basis for weighting PS snow cover patterns from years with more similar meteorological conditions and snow cover anomalies. This should be a topic for future research.

Relative to the probabilistic downscaling, the RF downscaling both 1) classified 3 m snow presence and absence using machine learning inference that was provided additional context about the terrain and fSCA evolution, and 2) corrected for coarser scale fSCA biases. To test which was the dominant cause of F1 score improvements, the bias-corrected MODIS fSCA from the RF downscaling was supplied to the probabilistic downscaling approach and used again to estimate 3 m snow cover. In all domains except GIN, this improved the distribution of F1 scores relative to both the probabilistic and RF downscalings (Fig. S20). This suggested that the fSCA bias-corrections were the primary driver of model improvement for the RF downscaling, and in most cases, assuming spatially repeatable snow cover patterns within the footprints of coarser resolution fSCA retrievals performed well.

These results show that the terrain-based downscaling benchmark used a methodology that could work well but was hindered by fSCA biases and terrain indices that did not fully explain the pattern of spring snow cover. For example, this approach performed best when using a weighting factor that prescribed the spatial difference in solar exposure and the resulting pattern of snowmelt as the dominant descriptor of the timing and location of snow disappearance (Fig. 4, $w = 0.75$). This was counter to Cristea et al. (2017), who found that snow cover was downscaled best when the weighting factor was changed from domain to domain, the best overall average resulting from an equal weighting ($w = 0.50$) of the impact of snow accumulation and melt patterns. While the impact of solar radiation has known impacts on the spatial pattern of snowmelt rates (e.g., Lundquist and Flint, 2006; Marks et al., 2002; Musselman et al., 2012; Pohl et al., 2006), the timing of snow disappearance is commonly found to be dictated more by the spatial pattern of snow accumulation (Dickerson-Lange et al., 2017; Egli et al., 2012; Egli and Jonas, 2009; Liston, 2004; Luce et al., 1998). In fact, using the same PS snow cover data used by this study, Pflug et al. (2024) found that spatially variable snowmelt rates resulted in little-to-no improvement to spring SWE estimates, relative to assuming spatially homogeneous snowmelt. We hypothesize that the best-performing SVI map used by the terrain-based downscaling benchmark implicitly accounted for spatial autocorrelation and alternative snow depletion and accumulation processes such as preferential deposition, sublimation, and snow holding capacity on steeply sloped terrain (Bernhardt and Schulz, 2010; Currier and Lundquist, 2018; Dadic et al., 2010; Trujillo et al., 2009; Winstral et al., 2013) and canopy effects like interception, shading, and local heat fluxes (Broxton et al., 2015; Currier and Lundquist, 2018; Dickerson-Lange et al., 2017; Lundquist et al., 2013; Mazzotti et al., 2019; Musselman et al., 2012).

Since both fSCA biases and 3 m snow cover patterns often had annually repeatable characteristics, future research should investigate whether an improved terrain-based snow pattern and an fSCA bias-correction could be calculated using information about the terrain, landcover, and PS observations from one or a limited number of years, and whether these relationships can be used to derive a snow pattern reference to downscale snow cover in surrounding areas without PS observations.

5.4. Study limitations and recommendations

Coarser resolution fSCA estimates from MODIS and VIIRS were biased consistently in locations where the satellite footprints had significant overlap with forested locations, making the RF downscaling important in those locations (Fig. 3). Additionally, due to the sensor point spread function, off-nadir viewing angles, parallax effects, and topographic shading, the area actually viewed by a MODIS or VIIRS retrieval can deviate from the assumed grid by an amount orders of magnitudes greater than the 3 m PS resolutions. For example, using an idealized approximation of the MODIS point spread function and assumption that the off-nadir viewing angle is in the exact same direction as the terrain slope, a MODIS pixel with a 15-degree

https://doi.org/10.5194/egusphere-2026-4850
Preprint. Discussion started: 20 August 2026

off-nadir viewing angle looking at a 30-degree slope could have more than half of its signal contributed by areas outside the nominal grid cell (Table S2). Future research could use this information as a basis for filtering retrievals with potentially high biases, or identifying portions of the landscape that may be more difficult to observe (e.g., Fig. 7, hatched regions).

It is also possible that fSCA biases could have been driven by gap-filling NDSI estimates using the most-recent prior cloud-free retrieval, the domains focused on in this study centered around small domains where spring cloud cover was less frequent than many locations (Pflug et al., 2024). As a result, we were unable to find any impact to the F1 score driven by the period of time elapsed between the PS comparison date and the prior cloud-free date observed by HLS (Fig. S19). However, future work could consider adding more robust cloud gap-filling procedures, and approaches designed to bias-correct fSCA estimates prior to downscaling snow cover (e.g., Dong et al., 2020; Premier et al., 2021; Woodruff and Qualls, 2019).

The linear NDSI to fSCA conversion used for MODIS and VIIRS (Salomonson and Appel, 2006, 2004) was also applied to the HLS data to maintain as much consistency as possible between the different sensors. However, this conversion was derived using binary snow cover processed from Landsat retrievals, which is part of the HLS dataset. This circuity between using Landsat to both train the NDSI to fSCA conversion and predict fSCA could have increased the frequency of fully snow-covered and snow-absent estimates for the HLS dataset. To test this, the snow covered area and grain size (SCAG; Painter et al., 2009) spectral unmixing approach was also used to convert the HLS retrievals to estimates of fSCA. Relative to PS snow cover that was coarsened to the HLS resolution, SCAG-based fSCA had improved spatial patterns of snow cover frequency, largely driven by decreases in snow cover in grid cells near the forest canopy (Figs. S21 and S22). However, the SCAG approach resulted in worse temporal coefficients of correlation across each domain, relative to the NDSI to fSCA conversion (e.g., Salomonson and Appel, 2006), and had similar absolute and relative biases (Table S3). These errors were likely minimal given that the errors from fSCA biases were typically outweighed by the impact of the domains, years, and downscaling approach.

PS snow cover maps may have been subject to uncertainties related to retrieval errors like sun glint and biases from the canopy edge. However, these snow cover maps the highest-accuracy and finest-resolution estimates of snow cover, as compared to airborne lidar (Pflug et al., 2024; Yang et a., 2023). Although the terrain-based downscaling parameters were calibrated to best match PS snow cover, it is possible that the downscaling approaches explicitly including PS snow cover from other years may have artificially increased the F1 score as PS snow cover biases could have persisted from year to year. However, PS observations serve as a higher accuracy and fully distributed benchmark for evaluating downscaled snow cover performance than alternative observations such as field observations. These retrievals are also much more frequent, globally distributed, and are more cost-effective than airborne lidar observations.

Finally, this study showed that while the downscaling approach and fSCA data source were important drivers of the accuracy of downscaled snow cover maps (in that order), results were variable across the different domains and years. Therefore, future research should expand to more locations and years. We also focused on only three snow cover downscaling approaches. While other approaches were investigated, we found that the three approaches focused on here bounded the potential range of accuracies well and used many common inputs (Fig. 2). This study is not intended to make sweeping statements about all downscaling procedures but instead demonstrate the relative contribution of finer-resolution snow cover data, where and when available, and the interaction with the accuracy of coarser resolution fSCA estimates across various years and montane domains.

6. Conclusions

Snow cover at fine spatial scales is challenging to observe and model. Recent observations from PlanetScope (PS) commercial remote sensing retrievals have demonstrated the capability of mapping snow cover at 3 m spatial resolutions in

https://doi.org/10.5194/egusphere-2026-4850
Preprint. Discussion started: 20 August 2026

complex terrain. Provided historical context from PS snow cover maps, we test whether historical snow cover can be downscaled from coarser resolution publicly accessible estimates of fractional snow-covered area from MODIS (500 m resolutions), VIIRS (375 m), and HLS (30 m) in montane meadows.

Provided three published downscaling approaches, the accuracy of 3 m downscaled snow cover maps varied as a function of 1) the domain and year, 2) the downscaling approach, and 3) the accuracy of the fSCA observation, in that order. On dates experiencing spring snowmelt, the approaches using historical PS snow cover observations outperformed the approach downscaling snow cover using terrain indices. This was particularly the case when downscaling from the coarser resolution fSCA estimates from MODIS and VIIRS. The best-performing downscaling approach tested here used a random forest machine learning model, which demonstrated the capability to correct fSCA biases that repeated annually for each MODIS, VIIRS, and HLS pixel. However, HLS observed snow cover at spatial resolutions that approached to scales at which snow cover in adjacent 3 m pixels tended to disappear at similar times. Therefore, HLS fSCA was better able to observe the explicit pattern of snow presence and absence, resulting in snow cover observations that benefitted from snow cover downscaling approaches less. As a result, fractional snow cover from HLS downscaled using the simpler terrain-based approach was comparable in performance to snow cover downscaled from MODIS and VIIRS using context from PS snow cover maps in other years. The results above suggest that the most practical approach for estimating fine-scale spring snow distribution depends on the application, and whether the economical and computational cost of accessing and processing commercial data sources justifies the improvements to snow cover estimates.

Author contributions

JP performed the snow cover downscaling tests and wrote the manuscript draft. KY and NC provided guidance on the PS-based snow cover mapping approach, and NC provided details about the terrain-based downscaling approach. All coauthors assisted with project planning and manuscript revisions.

Competing interests

One author is a member of The Cryosphere editorial board.

Code and data availability

PS retrievals can be accessed through PlanetLabs. The Commercial Smallsat Data Acquisition vendor page provides more information on data access (https://www.earthdata.nasa.gov/esds/csda/csda-vendor-planet). The PS snow cover maps, and the scripts used to process these snow cover estimates, are provided by Pflug et al. (2024). Cloud gap-filled NDSI from MODIS and VIIRS, and ASO digital elevation models can be accessed from the National Snow and Ice Data Center's Distributed Active Archive Center (https://nsidc.org/data/mod10a1f/versions/61, https://nsidc.org/data/vnp10a1f/versions/1, and https://nsidc.org/data/aso_3m_pcdtm/versions/1). Additional digital elevation models were accessed from the USGS's 3D Elevation Program (https://www.usgs.gov/3d-elevation-program). All terrain data and downscaled snow cover maps are provided at http://www.hydroshare.org/resource/fc2abc98881c4ea0a5e84856f3f5c09a (Pflug J.M., 2025a) and the scripts used to downscale snow cover estimates are accessible at https://doi.org/10.5281/zenodo.17516632 (Pflug, J.M., 2025b).

Financial support

https://doi.org/10.5194/egusphere-2026-4850
Preprint. Discussion started: 20 August 2026

The authors thank funding and support from the Commercial Smallsat Data Acquisition program, NASA Terrestrial Hydrology program, and NASA Grants 80NSSC23K0004 and 80NSSC24K0050.

References

Aalstad, K., Westermann, S., Bertino, L., 2020. Evaluating satellite retrieved fractional snow-covered area at a high-Arctic site using terrestrial photography. Remote Sens. Environ. 239, 111618. https://doi.org/10.1016/j.rse.2019.111618

Aas, K.S., Gisnås, K., Westermann, S., Berntsen, T.K., 2017. A Tiling Approach to Represent Subgrid Snow Variability in Coupled Land Surface–Atmosphere Models. J. Hydrometeorol. 18, 49–63. https://doi.org/10.1175/JHM-D-16-0026.1

Andreadis, K.M., Lettenmaier, D.P., 2006. Assimilating remotely sensed snow observations into a macroscale hydrology model. Adv. Water Resour. 29, 872–886. https://doi.org/10.1016/j.advwatres.2005.08.004

Arsenault, K.R., Houser, P.R., De Lannoy, G.J.M., 2014. Evaluation of the MODIS snow cover fraction product. Hydrol. Process. 28, 980–998. https://doi.org/10.1002/hyp.9636

Bair, E.H., Dozier, J., Rittger, K., Stillinger, T., Kleiber, W., Davis, R.E., 2023. How do tradeoffs in satellite spatial and temporal resolution impact snow water equivalent reconstruction? The Cryosphere 17, 2629–2643. https://doi.org/10.5194/tc-17-2629-2023

Bennett, K.E., Cherry, J.E., Balk, B., Lindsey, S., 2019. Using MODIS estimates of fractional snow cover area to improve streamflow forecasts in interior Alaska. Hydrol. Earth Syst. Sci. 23, 2439–2459. https://doi.org/10.5194/hess-23-2439-2019

Bernhardt, M., Schulz, K., 2010. SnowSlide: A simple routine for calculating gravitational snow transport. Geophys. Res. Lett. 37. https://doi.org/10.1029/2010GL043086

Bisht, G., Riley, W.J., Wainwright, H.M., Dafflon, B., Yuan, F., Romanovsky, V.E., 2018. Impacts of microtopographic snow redistribution and lateral subsurface processes on hydrologic and thermal states in an Arctic polygonal ground ecosystem: a case study using ELM-3D v1.0. Geosci. Model Dev. 11, 61–76. https://doi.org/10.5194/gmd-11-61-2018

Blöschl, G., 1999. Scaling issues in snow hydrology. Hydrol. Process. 13, 2149–2175. https://doi.org/10.1002/(SICI)1099-1085(199910)13:14/15<2149::AID-HYP847>3.0.CO;2-8

Boardman, E.N., Fountain, A.G., Boardman, J.W., Painter, T.H., Burgess, E.W., Wilson, L., Harpold, A.A., 2025. Wind and topography underlie correlation between seasonal snowpack, mountain glaciers, and late-summer streamflow. The Cryosphere 19, 3193–3225. https://doi.org/10.5194/tc-19-3193-2025

Brauchli, T., Trujillo, E., Huwald, H., Lehning, M., 2017. Influence of Slope-Scale Snowmelt on Catchment Response Simulated With the Alpine3D Model. Water Resour. Res. 53, 10723–10739.

Breckheimer, I.K., Theobald, E.J., Cristea, N.C., Wilson, A.K., Lundquist, J.D., Rochefort, R.M., HilleRisLambers, J., 2020. Crowd-sourced data reveal social–ecological mismatches in phenology driven by climate. Front. Ecol. Environ. 18, 76–82. https://doi.org/10.1002/fee.2142

Breen, C., Vuyovich, C., Odden, J., Hall, D., Prugh, L., 2023. Evaluating MODIS snow products using an extensive wildlife camera network. Remote Sens. Environ. 295, 113648. https://doi.org/10.1016/j.rse.2023.113648

Broxton, P.D., Harpold, A.A., Biederman, J.A., Troch, P.A., Molotch, N.P., Brooks, P.D., 2015. Quantifying the effects of vegetation structure on snow accumulation and ablation in mixed-conifer forests. Ecohydrology 8, 1073–1094. https://doi.org/10.1002/eco.1565

Cannistra, A.F., Shean, D.E., Cristea, N.C., 2021. High-resolution CubeSat imagery and machine learning for detailed snow-covered area. Remote Sens. Environ. 258, 112399. https://doi.org/10.1016/j.rse.2021.112399

https://doi.org/10.5194/egusphere-2026-4850
Preprint. Discussion started: 20 August 2026

Clark, M.P., Hendrikx, J., Slater, A.G., Kavetski, D., Anderson, B., Cullen, N.J., Kerr, T., Hreinsson, E.Ö., Woods, R.A., 2011. Representing spatial variability of snow water equivalent in hydrologic and land-surface models: A review. Water Resour. Res. 47. https://doi.org/10.1029/2011WR010745

Clark, M.P., Slater, A.G., Barrett, A.P., Hay, L.E., McCabe, G.J., Rajagopalan, B., Leavesley, G.H., 2006. Assimilation of snow covered area information into hydrologic and land-surface models. Adv. Water Resour. 29, 1209–1221. https://doi.org/10.1016/j.advwatres.2005.10.001

Claverie, M., Ju, J., Masek, J.G., Dungan, J.L., Vermote, E.F., Roger, J.-C., Skakun, S.V., Justice, C., 2018. The Harmonized Landsat and Sentinel-2 surface reflectance data set. Remote Sens. Environ. 219, 145–161. https://doi.org/10.1016/j.rse.2018.09.002

Cristea, N.C., Breckheimer, I., Raleigh, M.S., HilleRisLambers, J., Lundquist, J.D., 2017. An evaluation of terrain-based downscaling of fractional snow covered area data sets based on LiDAR-derived snow data and orthoimagery. Water Resour. Res. 53, 6802–6820. https://doi.org/10.1002/2017WR020799

Crumley, R.L., Bachand, C.L., Bennett, K.E., 2024. Snow Distribution Patterns Revisited: A Physics-Based and Machine Learning Hybrid Approach to Snow Distribution Mapping in the Sub-Arctic. Water Resour. Res. 60, e2023WR036180. https://doi.org/10.1029/2023WR036180

Currier, W.R., Lundquist, J.D., 2018. Snow Depth Variability at the Forest Edge in Multiple Climates in the Western United States. Water Resour. Res. 54, 8756–8773. https://doi.org/10.1029/2018WR022553

Czyzowska-Wisniewski, E.H., van Leeuwen, W.J.D., Hirschboeck, K.K., Marsh, S.E., Wisniewski, W.T., 2015. Fractional snow cover estimation in complex alpine-forested environments using an artificial neural network. Remote Sens. Environ. 156, 403–417. https://doi.org/10.1016/j.rse.2014.09.026

Dadic, R., Mott, R., Lehning, M., Burlando, P., 2010. Wind influence on snow depth distribution and accumulation over glaciers. J. Geophys. Res. Earth Surf. 115, F01012. https://doi.org/10.1029/2009JF001261

Deems, J.S., Fassnacht, S.R., Elder, K.J., 2008. Interannual Consistency in Fractal Snow Depth Patterns at Two Colorado Mountain Sites. J. Hydrometeorol. 9, 977–988. https://doi.org/10.1175/2008JHM901.1

Deems, J.S., Fassnacht, S.R., Elder, K.J., 2006. Fractal Distribution of Snow Depth from Lidar Data. J. Hydrometeorol. 7, 285–297. https://doi.org/10.1175/JHM487.1

Dickerson-Lange, S.E., Gersonde, R.F., Hubbart, J.A., Link, T.E., Nolin, A.W., Perry, G.H., Roth, T.R., Wayand, N.E., Lundquist, J.D., 2017. Snow disappearance timing is dominated by forest effects on snow accumulation in warm winter climates of the Pacific Northwest, United States. Hydrol. Process. 31, 1846–1862. https://doi.org/10.1002/hyp.11144

Dong, J., Crow, W.T., Tobin, K.J., Cosh, M.H., Bosch, D.D., Starks, P.J., Seyfried, M., Collins, C.H., 2020. Comparison of microwave remote sensing and land surface modeling for surface soil moisture climatology estimation. Remote Sens. Environ. 242, 111756. https://doi.org/10.1016/j.rse.2020.111756

Egli, L., Jonas, T., 2009. Hysteretic dynamics of seasonal snow depth distribution in the Swiss Alps. Geophys. Res. Lett. 36. https://doi.org/10.1029/2008GL035545

Egli, L., Jonas, T., Grünewald, T., Schirmer, M., Burlando, P., 2012. Dynamics of snow ablation in a small Alpine catchment observed by repeated terrestrial laser scans. Hydrol. Process. 26, 1574–1585.

Faria, D.A., Pomeroy, J.W., Essery, R.L.H., 2000. Effect of covariance between ablation and snow water equivalent on depletion of snow-covered area in a forest. Hydrol. Process. 14, 2683–2695. https://doi.org/10.1002/1099-1085(20001030)14:15<2683::AID-HYP86>3.0.CO;2-N

https://doi.org/10.5194/egusphere-2026-4850
Preprint. Discussion started: 20 August 2026

Ford, K.R., Ettinger, A.K., Lundquist, J.D., Raleigh, M.S., Lambers, J.H.R., 2013. Spatial Heterogeneity in Ecologically Important Climate Variables at Coarse and Fine Scales in a High-Snow Mountain Landscape. PLOS ONE 8, e65008. https://doi.org/10.1371/journal.pone.0065008

Frazier, A.E., Hemingway, B.L., 2021. A Technical Review of Planet Smallsat Data: Practical Considerations for Processing and Using PlanetScope Imagery. Remote Sens. 13, 3930. https://doi.org/10.3390/rs13193930

Gunnarsson, A., Garðarsson, S.M., Sveinsson, Ó.G.B., 2019. Icelandic snow cover characteristics derived from a gap-filled MODIS daily snow cover product. Hydrol. Earth Syst. Sci. 23, 3021–3036. https://doi.org/10.5194/hess-23-3021-2019

Hall, D.K., Riggs, G.A., 2020. MODIS/Terra CGF Snow Cover Daily L3 Global 500m SIN Grid, Version 61. https://doi.org/10.5067/MODIS/MOD10A1F.061

Hall, D.K., Riggs, G.A., DiGirolamo, N.E., Román, M.O., 2019. Evaluation of MODIS and VIIRS cloud-gap-filled snow-cover products for production of an Earth science data record. Hydrol. Earth Syst. Sci. 23, 5227–5241. https://doi.org/10.5194/hess-23-5227-2019

Hall, D.K., Riggs, G.A., Salomonson, V.V., 1995. Development of methods for mapping global snow cover using moderate resolution imaging spectroradiometer data. Remote Sens. Environ. 54, 127–140. https://doi.org/10.1016/0034-4257(95)00137-P

Heidemann, H.K., 2012. Lidar base specification (No. 11-B4), Techniques and Methods. U.S. Geological Survey. https://doi.org/10.3133/tm11B4

Helbig, N., Bühler, Y., Eberhard, L., Deschamps-Berger, C., Gascoin, S., Dumont, M., Revuelto, J., Deems, J.S., Jonas, T., 2021. Fractional snow-covered area: scale-independent peak of winter parameterization. The Cryosphere 15, 615–632. https://doi.org/10.5194/tc-15-615-2021

Helfricht, K., Schöber, J., Schneider, K., Sailer, R., Kuhn, M., 2014. Interannual persistence of the seasonal snow cover in a glacierized catchment. J. Glaciol. 60, 889–904. https://doi.org/10.3189/2014JoG13J197

John, A., Cannistra, A.F., Yang, K., Tan, A., Shean, D., Hille Ris Lambers, J., Cristea, N., 2022. High-Resolution Snow-Covered Area Mapping in Forested Mountain Ecosystems Using PlanetScope Imagery. Remote Sens. 14, 3409. https://doi.org/10.3390/rs14143409

Kostadinov, T.S., Schumer, R., Hausner, M., Bormann, K.J., Gaffney, R., McGwire, K., Painter, T.H., Tyler, S., Harpold, A.A., 2019. Watershed-scale mapping of fractional snow cover under conifer forest canopy using lidar. Remote Sens. Environ. 222, 34–49. https://doi.org/10.1016/j.rse.2018.11.037

Krogh, S.A., Pomeroy, J.W., 2021. Simulating site-scale permafrost hydrology: Sensitivity to modelling decisions and air temperature. J. Hydrol. 602, 126771. https://doi.org/10.1016/j.jhydrol.2021.126771

Kronholm, K., Schweizer, J., 2003. Snow stability variation on small slopes. Cold Reg. Sci. Technol., ISSW 2002: International Snow Science Workshop 37, 453–465. https://doi.org/10.1016/S0165-232X(03)00084-3

Lehning, M., Völksch, I., Gustafsson, D., Nguyen, T.A., Stähli, M., Zappa, M., 2006. ALPINE3D: a detailed model of mountain surface processes and its application to snow hydrology. Hydrol. Process. 20, 2111–2128. https://doi.org/10.1002/hyp.6204

Liston, G.E., 2004. Representing Subgrid Snow Cover Heterogeneities in Regional and Global Models. J. Clim. 17, 1381–1397. https://doi.org/10.1175/1520-0442(2004)017<1381:RSSCHI>2.0.CO;2

Liston, G.E., Elder, K., 2006. A Distributed Snow-Evolution Modeling System (SnowModel). J. Hydrometeorol. 7, 1259–1276. https://doi.org/10.1175/JHM548.1

https://doi.org/10.5194/egusphere-2026-4850
Preprint. Discussion started: 20 August 2026

Litaor, M.I., Williams, M., Seastedt, T.R., 2008. Topographic controls on snow distribution, soil moisture, and species diversity of herbaceous alpine vegetation, Niwot Ridge, Colorado. J. Geophys. Res. Biogeosciences 113. https://doi.org/10.1029/2007JG000419

Liu, C., Li, Z., Zhang, P., Zeng, J., Gao, S., Zheng, Z., 2020. An Assessment and Error Analysis of MOD10A1 Snow Product Using Landsat and Ground Observations Over China During 2000–2016. IEEE J. Sel. Top. Appl. Earth Obs. Remote Sens. 13, 1467–1478. https://doi.org/10.1109/JSTARS.2020.2983550

Liu, Y., Peters-Lidard, C.D., Kumar, S.V., Foster, J.L., Shaw, M., Tian, Y., Fall, G.M., 2013. Assimilating satellite-based snow depth and snow cover products for improving snow predictions in Alaska. Adv. Water Resour. 54, 208–227. https://doi.org/10.1016/j.advwatres.2013.02.005

Luce, C.H., Tarboton, D.G., 2004. The application of depletion curves for parameterization of subgrid variability of snow. Hydrol. Process. 18, 1409–1422. https://doi.org/10.1002/hyp.1420

Luce, C.H., Tarboton, D.G., Cooley, K.R., 1998. The influence of the spatial distribution of snow on basin-averaged snowmelt. Hydrol. Process. 12, 1671–1683. https://doi.org/10.1002/(SICI)1099-1085(199808/09)12:10/11<1671::AID-HYP688>3.0.CO;2-N

Lundquist, J.D., Dickerson-Lange, S.E., Lutz, J.A., Cristea, N.C., 2013. Lower forest density enhances snow retention in regions with warmer winters: A global framework developed from plot-scale observations and modeling. Water Resour. Res. 49, 6356–6370. https://doi.org/10.1002/wrcr.20504

Lundquist, J.D., Flint, A.L., 2006. Onset of Snowmelt and Streamflow in 2004 in the Western United States: How Shading May Affect Spring Streamflow Timing in a Warmer World. J. Hydrometeorol. 7, 1199–1217. https://doi.org/10.1175/JHM539.1

Magoun, A.J., Robards, M.D., Packila, M.L., Glass, T.W., 2017. Detecting snow at the den-site scale in wolverine denning habitat. Wildl. Soc. Bull. 41, 381–387. https://doi.org/10.1002/wsb.765

Mahanthege, S., Kleiber, W., Rittger, K., Rajagopalan, B., Brodzik, M.J., Bair, E., 2024. A Spatially-Distributed Machine Learning Approach for Fractional Snow Covered Area Estimation. Water Resour. Res. 60, e2023WR036162. https://doi.org/10.1029/2023WR036162

Margulis, S.A., Girotto, M., Cortés, G., Durand, M., 2015. A Particle Batch Smoother Approach to Snow Water Equivalent Estimation. J. Hydrometeorol. 16, 1752–1772. https://doi.org/10.1175/JHM-D-14-0177.1

Marks, D., Winstral, A., Seyfried, M., 2002. Simulation of terrain and forest shelter effects on patterns of snow deposition, snowmelt and runoff over a semi-arid mountain catchment. Hydrol. Process. 16, 3605–3626. https://doi.org/10.1002/hyp.1237

Mazzotti, G., Currier, W.R., Deems, J.S., Pflug, J.M., Lundquist, J.D., Jonas, T., 2019. Revisiting Snow Cover Variability and Canopy Structure Within Forest Stands: Insights From Airborne Lidar Data. Water Resour. Res. 55, 6198–6216. https://doi.org/10.1029/2019WR024898

Mazzotti, G., Essery, R., Moeser, C.D., Jonas, T., 2020. Resolving Small-Scale Forest Snow Patterns Using an Energy Balance Snow Model With a One-Layer Canopy. Water Resour. Res. 56, e2019WR026129. https://doi.org/10.1029/2019WR026129

Mendoza, P.A., Musselman, K.N., Revuelto, J., Deems, J.S., López-Moreno, J.I., McPhee, J., 2020. Interannual and Seasonal Variability of Snow Depth Scaling Behavior in a Subalpine Catchment. Water Resour. Res. 56, e2020WR027343. https://doi.org/10.1029/2020WR027343

Miller, Z.S., Peitzsch, E.H., Sproles, E.A., Birkeland, K.W., Palomaki, R.T., 2022. Assessing the seasonal evolution of snow depth spatial variability and scaling in complex mountain terrain. The Cryosphere 16, 4907–4930. https://doi.org/10.5194/tc-16-4907-2022

Mott, R., Lehning, M., 2010. Meteorological Modeling of Very High-Resolution Wind Fields and Snow Deposition for Mountains. J. Hydrometeorol. 11, 934–949. https://doi.org/10.1175/2010JHM1216.1

Musselman, K.N., Molotch, N.P., Margulis, S.A., Kirchner, P.B., Bales, R.C., 2012. Influence of canopy structure and direct beam solar irradiance on snowmelt rates in a mixed conifer forest. Agric. For. Meteorol. 161, 46–56. https://doi.org/10.1016/j.agrformet.2012.03.011

Oldfather, M.F., Elmendorf, S.C., Van Cleemput, E., Henn, J.J., Huxley, J.D., White, C.T., Humphries, H.C., Spasojevic, M.J., Suding, K.N., Emery, N.C., 2024. Divergent community trajectories with climate change across a fine-scale gradient in snow depth. J. Ecol. 112, 126–137. https://doi.org/10.1111/1365-2745.14223

Ortner, G., Bründl, M., Kropf, C.M., Röösli, T., Bühler, Y., Bresch, D.N., 2023. Large-scale risk assessment on snow avalanche hazard in alpine regions. Nat. Hazards Earth Syst. Sci. 23, 2089–2110. https://doi.org/10.5194/nhess-23-2089-2023

Painter, T., Bormann, K., 2020. ASO L4 Lidar Point Cloud Digital Terrain Model 3m UTM Grid, Version 1. https://doi.org/10.5067/2EHMWG4IT76O

Painter, T.H., Berisford, D.F., Boardman, J.W., Bormann, K.J., Deems, J.S., Gehrke, F., Hedrick, A., Joyce, M., Laidlaw, R., Marks, D., Mattmann, C., McGurk, B., Ramirez, P., Richardson, M., Skiles, S.M., Seidel, F.C., Winstral, A., 2016. The Airborne Snow Observatory: Fusion of scanning lidar, imaging spectrometer, and physically-based modeling for mapping snow water equivalent and snow albedo. Remote Sens. Environ. 184, 139–152. https://doi.org/10.1016/j.rse.2016.06.018

Painter, T.H., Rittger, K., McKenzie, C., Slaughter, P., Davis, R.E., Dozier, J., 2009. Retrieval of subpixel snow covered area, grain size, and albedo from MODIS. Remote Sens. Environ. 113, 868–879. https://doi.org/10.1016/j.rse.2009.01.001

Pflug, J.M., Hughes, M., Lundquist, J.D., 2021. Downscaling snow deposition using historic snow depth patterns: Diagnosing limitations from snowfall biases, winter snow losses, and interannual snow pattern repeatability. Water Resour. Res. e2021WR029999. https://doi.org/10.1029/2021WR029999

Pflug, J.M., Kumar, S.V., Hall, D.K., Riggs, G.A., Konapala, G., Whitney, K.M., Wrzesien, M.L., Nie, W., Sun, Z., Arsenault, K.R., 2025. Efficient and Regionally Transferable Snow Water Equivalent Estimation Using a Long Short-Term Memory Network. J. Geophys. Res. Mach. Learn. Comput. 2, e2025JH000593. https://doi.org/10.1029/2025JH000593

Pflug, J.M., Lundquist, J.D., 2020. Inferring Distributed Snow Depth by Leveraging Snow Pattern Repeatability: Investigation Using 47 Lidar Observations in the Tuolumne Watershed, Sierra Nevada, California. Water Resour. Res. 56, e2020WR027243. https://doi.org/10.1029/2020WR027243

Pflug, J.M., Margulis, S.A., Lundquist, J.D., 2022. Inferring watershed-scale mean snowfall magnitude and distribution using multidecadal snow reanalysis patterns and snow pillow observations. Hydrol. Process. 36, e14581.

Pflug, J.M., Yang, K., Cristea, N., Boudreau, E.T., Vuyovich, C.M., Kumar, S.V., 2024. Using Commercial Satellite Imagery to Reconstruct 3 m and Daily Spring Snow Water Equivalent. Water Resour. Res. 60, e2024WR037983. https://doi.org/10.1029/2024WR037983

Pfohl, S., Marsh, P., Pietroniro, A., 2006. Spatial–temporal variability in solar radiation during spring snowmelt. Hydrol. Res. 37, 1–19. https://doi.org/10.2166/nh.2006.0001

Premier, V., Marin, C., Notarnicola, C., Bruzzone, L., 2021a. A Multisource Statistical Method to Downscale Snow Cover Fraction in Mountain Regions, in: 2021 IEEE International Geoscience and Remote Sensing Symposium IGARSS. Presented at the 2021 IEEE International Geoscience and Remote Sensing Symposium IGARSS, pp. 5481–5484. https://doi.org/10.1109/IGARSS47720.2021.9554898

https://doi.org/10.5194/egusphere-2026-4850
Preprint. Discussion started: 20 August 2026

Premier, V., Marin, C., Steger, S., Notarnicola, C., Bruzzone, L., 2021b. A Novel Approach Based on a Hierarchical Multiresolution Analysis of Optical Time Series to Reconstruct the Daily High-Resolution Snow Cover Area. IEEE J. Sel. Top. Appl. Earth Obs. Remote Sens. 14, 9223–9240. https://doi.org/10.1109/JSTARS.2021.3103585

Raleigh, M.S., Rittger, K., Moore, C.E., Henn, B., Lutz, J.A., Lundquist, J.D., 2013. Ground-based testing of MODIS fractional snow cover in subalpine meadows and forests of the Sierra Nevada. Remote Sens. Environ. 128, 44–57. https://doi.org/10.1016/j.rse.2012.09.016

Revuelto, J., Alonso-González, E., Gascoin, S., Rodríguez-López, G., López-Moreno, J.I., 2021. Spatial Downscaling of MODIS Snow Cover Observations Using Sentinel-2 Snow Products. Remote Sens. 13, 4513. https://doi.org/10.3390/rs13224513

Reynolds, D.S., Pflug, J.M., Lundquist, J.D., 2021. Evaluating Wind Fields for Use in Basin-Scale Distributed Snow Models. Water Resour. Res. 57, e2020WR028536. https://doi.org/10.1029/2020WR028536

Riggs, G., Hall, D., Rom??n, M., 2019. VIIRS/NPP CGF Snow Cover Daily L3 Global 375m SIN Grid, Version 1. https://doi.org/10.5067/VIIRS/VNP10A1F.001

Riggs, G.A., Hall, D.K., Román, M.O., 2017. Overview of NASA's MODIS and Visible Infrared Imaging Radiometer Suite (VIIRS) snow-cover Earth System Data Records. Earth Syst. Sci. Data 9, 765–777. https://doi.org/10.5194/essd-9-765-2017

Rittger, K., Bormann, K.J., Bair, E.H., Dozier, J., Painter, T.H., 2021a. Evaluation of VIIRS and MODIS Snow Cover Fraction in High-Mountain Asia Using Landsat 8 OLI. Front. Remote Sens. 2. https://doi.org/10.3389/frsen.2021.647154

Rittger, K., Krock, M., Kleiber, W., Bair, E.H., Brodzik, M.J., Stephenson, T.R., Rajagopalan, B., Bormann, K.J., Painter, T.H., 2021b. Multi-sensor fusion using random forests for daily fractional snow cover at 30 m. Remote Sens. Environ. 264, 112608. https://doi.org/10.1016/j.rse.2021.112608

Salomonson, V.V., Appel, I., 2006. Development of the Aqua MODIS NDSI fractional snow cover algorithm and validation results. IEEE Trans. Geosci. Remote Sens. 44, 1747–1756. https://doi.org/10.1109/TGRS.2006.876029

Salomonson, V.V., Appel, I., 2004. Estimating fractional snow cover from MODIS using the normalized difference snow index. Remote Sens. Environ. 89, 351–360. https://doi.org/10.1016/j.rse.2003.10.016

Schirmer, M., Wirz, V., Clifton, A., Lehning, M., 2011. Persistence in intra-annual snow depth distribution: 1. Measurements and topographic control. Water Resour. Res. 47.

Schweizer, J., Kronholm, K., Jamieson, J.B., Birkeland, K.W., 2008. Review of spatial variability of snowpack properties and its importance for avalanche formation. Cold Reg. Sci. Technol., International Snow Science Workshop (ISSW) 2006 51, 253–272. https://doi.org/10.1016/j.coldregions.2007.04.009

Selkowitz, D.J., Forster, R.R., Caldwell, M.K., 2014. Prevalence of Pure Versus Mixed Snow Cover Pixels across Spatial Resolutions in Alpine Environments. Remote Sens. 6, 12478–12508. https://doi.org/10.3390/rs61212478

Shamir, E., Georgakakos, K.P., 2007. Estimating snow depletion curves for American River basins using distributed snow modeling. J. Hydrol. 334, 162–173. https://doi.org/10.1016/j.jhydrol.2006.10.007

Shirley, I., Uhlemann, S., Peterson, J., Bennett, K., Hubbard, S.S., Dafflon, B., 2025. Disentangling the Impacts of Microtopography and Shrub Distribution on Snow Depth in a Subarctic Watershed: Toward a Predictive Understanding of Snow Spatial Variability. J. Geophys. Res. Biogeosciences 130, e2024JG008604. https://doi.org/10.1029/2024JG008604

Sirguey, P., Mathieu, R., Arnaud, Y., 2009. Subpixel monitoring of the seasonal snow cover with MODIS at 250 m spatial resolution in the Southern Alps of New Zealand: Methodology and accuracy assessment. Remote Sens. Environ. 113, 160–181. https://doi.org/10.1016/j.rse.2008.09.008

https://doi.org/10.5194/egusphere-2026-4850
Preprint. Discussion started: 20 August 2026

Stillinger, T., Rittger, K., Raleigh, M.S., Michell, A., Davis, R.E., Bair, E.H., 2023. Landsat, MODIS, and VIIRS snow cover mapping algorithm performance as validated by airborne lidar datasets. The Cryosphere 17, 567–590. https://doi.org/10.5194/tc-17-567-2023

Sturm, M., Wagner, A.M., 2010. Using repeated patterns in snow distribution modeling: An Arctic example. Water Resour. Res. 46.

Trujillo, E., Ramírez, J.A., Elder, K.J., 2009. Scaling properties and spatial organization of snow depth fields in sub-alpine forest and alpine tundra. Hydrol. Process. 23, 1575–1590. https://doi.org/10.1002/hyp.7270

Trujillo, E., Ramírez, J.A., Elder, K.J., 2007. Topographic, meteorologic, and canopy controls on the scaling characteristics of the spatial distribution of snow depth fields. Water Resour. Res. 43.

Vögeli, C., Lehning, M., Wever, N., Bavay, M., 2016. Scaling Precipitation Input to Spatially Distributed Hydrological Models by Measured Snow Distribution. Front. Earth Sci. 4. https://doi.org/10.3389/feart.2016.00108

Winstral, A., Marks, D., Gurney, R., 2013. Simulating wind-affected snow accumulations at catchment to basin scales. Adv. Water Resour., Snow–Atmosphere Interactions and Hydrological Consequences 55, 64–79. https://doi.org/10.1016/j.advwatres.2012.08.011

Woodruff, C.D., Qualls, R.J., 2019. Recurrent Snowmelt Pattern Synthesis using Principal Component Analysis of Multi-Year Remotely Sensed Snow Cover. Water Resour. Res. 55, 6869–6885. https://doi.org/10.1029/2018WR024546

Xin, Q., Woodcock, C.E., Liu, J., Tan, B., Melloh, R.A., Davis, R.E., 2012. View angle effects on MODIS snow mapping in forests. Remote Sens. Environ. 118, 50–59. https://doi.org/10.1016/j.rse.2011.10.029

Yang, K., John, A., Shean, D., Lundquist, J.D., Sun, Z., Yao, F., Todoran, S., Cristea, N., 2023. High-resolution mapping of snow cover in montane meadows and forests using Planet imagery and machine learning. Front. Water 5.

Yang, K., Musselman, K.N., Rittger, K., Margulis, S.A., Painter, T.H., Molotch, N.P., 2021. Combining ground-based and remotely sensed snow data in a linear regression model for real-time estimation of snow water equivalent. Adv. Water Resour. 104075. https://doi.org/10.1016/j.advwatres.2021.104075

Zanaga, D., Van De Kerchove, R., Daems, D., De Keersmaecker, W., Brockmann, C., Kirches, G., Wevers, J., Cartus, O., Santoro, M., Fritz, S., Lesiv, M., Herold, M., Tsendbazar, N.-E., Xu, P., Ramoino, F., Arino, O., 2022. ESA WorldCover 10 m 2021 v200. https://doi.org/10.5281/zenodo.7254221